

Thesis

Ekaterina Avdeeva

University of Nebraska-Lincoln, USA

November 30, 2016

Abstract

This paper reviews

Contents

8	1	Introduction	2
9	1.1	Fundamental Particles and Interactions	4
10	1.2	Electroweak Interactions	6
11	1.3	Strong Interactions	9
12	1.4	Phyiscs of Proton-Proton Collisions	10
13	1.5	Open Questions of the Standard Model	12
14	2	$W\gamma$ Production Theory and Former Experimental Results	13
15	2.1	Electroweak Theory of the Standard Model	14
16	2.2	Cross Section and Luminosity	19
17	2.3	Standard Model $W\gamma$ Production	21
18	2.4	Anomalous $W\gamma$ Production	23
19	2.5	Measurements in the Past	26
20	3	Experimental Setup	28
21	3.1	Large Hadron Collider	29
22	3.2	Compact Muon Solenoid	32
23	3.2.1	Introduction	32
24	3.2.2	Magnet	33
25	3.2.3	Tracking System	33
26	3.2.4	Electromagnetic Calorimeter	33
27	3.2.5	Hadron Calorimeter	34
28	3.2.6	Muon System	34
29	3.2.7	Triggering and Data Aquisition	35
30	3.2.8	Event Reconstruction	36
31	4	CMS Tracker Alignment	38
32	4.1	Algorithm	39
33	4.2	Selected Results	44
34	5	$W\gamma$ Cross Section Measurement	45

35 1 Introduction

36 Elementary particle physics describes our world in terms of its smallest constituents, fundamen-
37 tal particles, and their interactions. Going from larger to smaller scales, substances around us
38 consist of molecules, molecules consist of atoms, in an atom, there is a nucleus made of neutrons
39 and protons and some number of electrons occupying their orbits around the nucleus. Protons
40 and neutrons have a structure while an electron is not known to have any structure, therefore,
41 an electron is an example of a particle which is considered to be fundamental.

42 Interactions of elementary particles are described by quantum field theories which incorporate
43 principles of the quantum mechanics and the special theory of relativity. The set of such theories,
44 including quantum elecrtrodynamics (QED), quantum chromodynamics (QCD) and the theory
45 of weak interactions is called the Standard Model (SM). It has been proven to be an accurate
46 description of interactions of elementary particles observed by now.

47 However, there are several experimental observations which are not described by the SM such
48 as gravity, dark matter, dark energy, matter/antimatter asymmetry and others. Therefore, the
49 SM is not the complete theory of particle interactions. There are several SM extensions offered by
50 theorists as well as radically new theories waiting for the experimental confirmation or disproof.

51 Some SM extensions and new theories predict the existence of heavy particles mass of which
52 possibly lies beyond experimentally reachable energies. The search of these particles is one of
53 the prioritized directions in particle physics. For such searches we need to reach higher ener-
54 gies than those which were probed before. One source of highly energetic elementary particles
55 is cosmic rays. The most energetic particles ever observed came from this source. However,
56 cosmic rays are totally uncontrollable and such highly energetic particles are rare. If we want
57 to produce a large number of particles at certain energies, we need to use a particle accelera-
58 tor. A large number of events at certain energy allows experimentalists to perform a statistical
59 analysis and increase the probability of finding a new particle if it exists in the given energy range.

60 Symmetric colliding beams is the most effective way to produce as heavy particles as possible
61 given the energies of the colliding particles. The Large Hadron Collider (LHC) is such a collider
62 with the highest energy in the world ever built. It can produce the most massive particles to
63 probe physics beyond the SM. It collides two proton beams with the several TeV of energy each.
64 The design center-of-mass energy of LHC is 14 TeV but it also probes several lower energy points
65 and may go higher.

66 Compact Muon Solenoid (CMS) is one of two general-purpose detectors at the LHC. It is
67 placed at one of six collision points. CMS has a wide physics program including searches for the
68 beyond SM (BSM) physics as well as the precision measurements of the SM parameters them-
69 selves.

70 In this dissertation the analysis of $pp \rightarrow W\gamma + X$ processes using leptonic decays of $W \rightarrow \ell\nu$
71 where $\ell = e, \mu$ is reported. The $W\gamma$ productions with leptonic W decays can go through one of
72 the following three processes: initial state radiation where a photon is produced from one of the
73 incoming partons, final state radiation where a photon is radiated off the charged lepton from
74 the W boson decay, and finally when a photon is produced via the triple gauge coupling (TGC)
75 where a photon is emitted from the W boson.

76 To search for the deviations from the SM, one would search for an anomalous TGC which
77 would be indicated by the enhance of the TGC production over the SM prediction.

78 The total and the differential cross section with respect to the photon transverse momentum
79 (P_T^γ) has been measured. The P_T^γ is sensitive to the potential anomalous TGC (aTGC) in the
80 high P_T^γ region. The disagreement between the measured and theoretically predicted differential
81 cross section at the higher P_T^γ end would be an indication of the possible presence of the aTGC.

90
91 The rest of this chapter gives general introductory information about the SM while chapter
92 2 concentrates on the theory of the SM and BSM $W\gamma$ production and also discusses previous
93 measurements of this process. Chapter 3 describes LHC and CMS in more details. Chapter
94 4 explaines on specific aspect of the CMS operation which is the tracker alignment. Finally,
95 chapter 5 describes the details of the measurement of this dissertation and reports the results.
96

97 1.1 Fundamental Particles and Interactions

98 The SM describes interactions of elementary particles. There are four fundamental interactions:
99 electromagnetic, strong, weak and gravitational. The gravity is not included into the SM but its
100 effect on particles is negligible compared to the other forces which makes it possible to develop a
101 theory of the particle physics and conduct experiments even without having the gravity included
102 into the model.

103 All fundamental elementary particles in the SM can be split into three categories by their
104 spins. There are fermions which possess spin $s=1/2$, there are gauge bosons which are also called
105 force mediators are vector particles ($s=1$) and there is the Higgs boson which is a scalar particle
106 ($s=0$).
107

108 The fermions are arranged into three generations, each generation consists of a quark with
109 charge $Q=+2/3$ (up, charm, and top quarks), a quark with $Q=-1/3$ (down, strange, and bottom
110 quarks), a charged lepton with $Q=-1$ (electron, muon, and tau-lepton) and a neutrino (electron,
111 muon, and tau neutrinos) which is electrically neutral. Each quark can carry any of three colors:
112 red, blue, or green. Additionally, each fermion has its antiparticle. Therefore, the total number
113 of fundamental fermions is $(6(\text{leptons}) + 6(\text{quarks}) \cdot 3(\text{colors})) \cdot 2(\text{to include antiparticles}) = 48$.
114

115 Corresponding particles in different generations have the same charges, spins and interaction
116 properties but masses of particles increase with a generation. These mass differences
117 lead to different decay properties because a particle A can decay to particles B and C only
118 if the mass of A $m_A > m_B + m_C$. Thus, an electron is a stable particle, a muon decays as
119 $\mu^- \rightarrow e^- + \bar{\nu}_e + \nu_\mu$, a tau-lepton, as the heaviest charged lepton, has the largest number of decay
120 channels: $\tau^- \rightarrow \mu^- + \bar{\nu}_\mu + \nu_\tau$, $\tau^- \rightarrow e^- + \bar{\nu}_e + \nu_\tau$, $\tau^- \rightarrow \nu_\tau + \text{quarks}$.
121

122 In addition to fermions, the SM includes gauge bosons which are mediators for the SM interactions.
123 A photon is a mediator for the electromagnetic interactions, a gluon is a mediator
124 for the strong interactions, and W^\pm and Z^0 bosons are mediators for the weak interactions. W^\pm
125 and Z^0 bosons are massive while a photon and a gluon are massless particles.
126

127 The last SM particle is the Higgs boson. The Higgs boson is a scalar neutral particle which
128 is playing a critical role in the electroweak symmetry breaking. The Higgs mechanism describes
129 how W and Z bosons become massive particles.
130

131 All the particles are summarized in Fig. 1. These and only these fundamental particles and
132 their antiparticles have been discovered by now. However, there are many composite particles
133 which are called hadrons. Hadrons can consist of three quarks (baryons), quark and antiquark
134 (meson), or three antiquarks (antibaryons). Hadrons always possess an integer charge.
135

136 Most of the particles are short-lived and decay within microseconds. The only stable particles
137 are protons and antiprotons, electrons and positrons, neutrinos and antineutrinos, photons,
138 and, in some sense, gluons. However, if a particle cannot decay, it does not mean that it would
139 live forever. There are many different kinds of reactions in which particles can disappear. An-
140 tiprotons and positrons would immediately annihilate with protons and electrons, photons can
141 be absorbed by charged particles, electrons and protons can scatter to produce neutrons and
142 neutrinos and many other reactions are possible.
143

144 In this dissertation a process is studied where quark and antiquark interact to produce a W
145 boson which then decay as $W^\pm \rightarrow e^\pm \nu_e (\bar{\nu}_e)$ or $W^\pm \rightarrow \mu^\pm \nu_\mu (\bar{\nu}_\mu)$. A photon is radiated off a
146 quark or antiquark, a charged lepton or a W boson. The most interesting mechanism out of three
147 is a radiation from a W boson because this is the triple gauge coupling where we potentially
148 can have a new physics. Therefore, the focus of this study is an interaction between a photon
149 and a W boson however many other SM particles are relevant too. Thus, a charged lepton and
150 a neutrino appear as the final state particles, a quark and an antiquark appear as initial state
151

152 particles and all fundamental particles except the Higgs boson participate in various background
 153 processes. Subsections 1.2-1.4, chapter 2 and [1] describe particle interactions in more details.

154

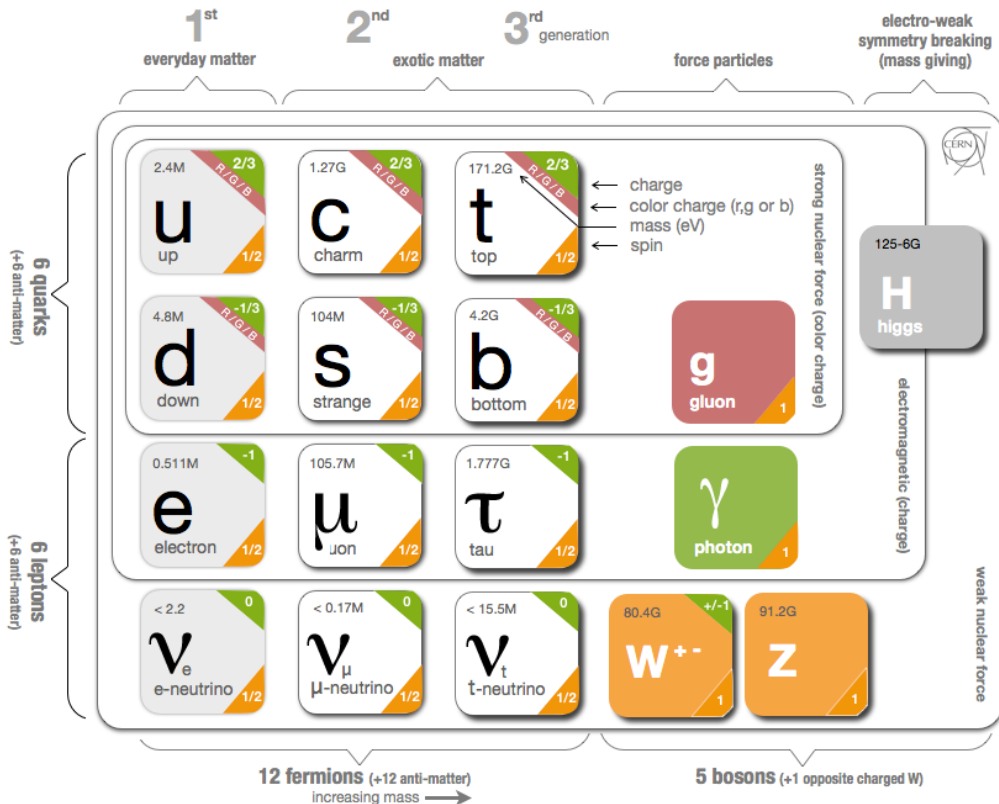


Figure 1: Standard Model Particles and Interactions. Source of the figure: [2].

155 **1.2 Electroweak Interactions**

156 All electrically charged particles participate in electromagnetic interactions. All electromagnetic
 157 interactions are mediated by a photon, a spin-one electrically neutral massless particle, and can
 158 be reduced to one elementary process (Fig. 2, left). This process represents an electron radiating
 159 or absorbing a photon. Although an electron is drawn in this figure, it can be any other charged
 160 particle as well. Such elementary process itself is forbidden by the energy conservation law but
 161 this element is a base of actual process (for example, Fig. 2, middle and right). Such graphical
 162 representations of the particle physics processes are called Feynman diagrams.

163

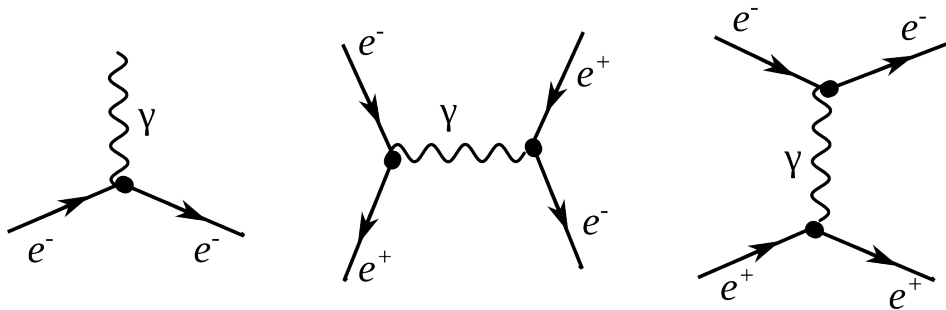


Figure 2: Electromagnetic interactions

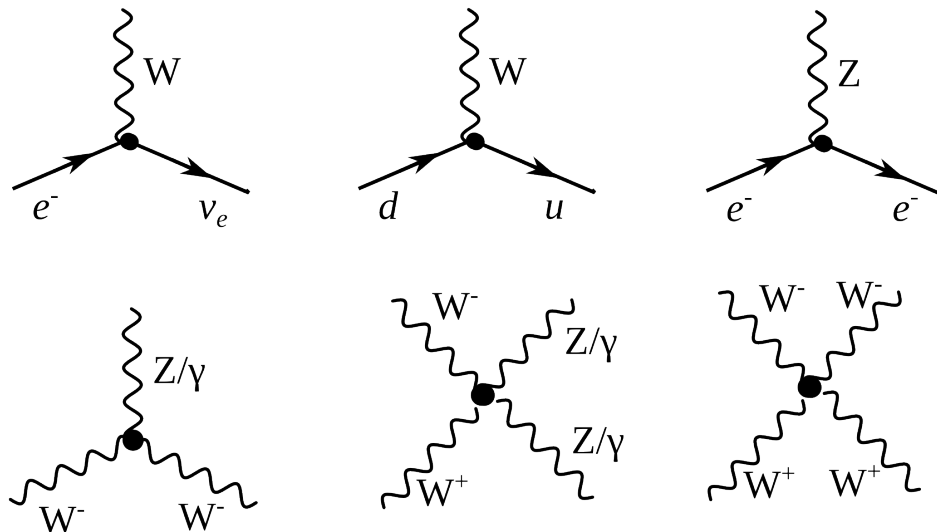


Figure 3: Weak elementary processes and gauge couplings

164 As for the weak interactions, there are two kinds of them: neutral (mediated by a Z boson)
 165 and charged (mediated by a W^\pm boson). Elementary processes with W and Z bosons are shown

in Fig. 3. Because the electric charge must be conserved at any vertex, a particle radiating or absorbing a W boson converts to a different particle. Thus, a charged lepton converts to a neutrino (or vice versa) as shown in Fig. 3, top left. Each lepton carries a lepton flavor number (Tab. 1). A lepton flavor number is conserved in any interaction, thus an electron radiating a W boson always converts to an electron neutrino, a muon converts to a muon neutrino etc.

171

Table 1: Lepton Flavor Number

particles	L_e	L_μ	L_τ
e^-, ν_e	+1	0	0
$e^+, \bar{\nu}_e$	-1	0	0
μ^-, ν_μ	0	+1	0
$\mu^+, \bar{\nu}_\mu$	0	-1	0
τ^-, ν_τ	0	0	+1
$\tau^+, \bar{\nu}_\tau$	0	0	-1

From top middle diagram in Fig. 3 we see that if a quark with $Q=-1/3$ enters, then a quark with $Q=+2/3$ escapes and, therefore, the flavor of the quark is changed. The charged weak interaction is the only interaction which changes a quark flavor. The probability of each of three quarks with $Q=+2/3$ to be born is determined by the Cabibbo Kobayashi Maskawa matrix and is the highest for the quark of the same generation as an initial state quark. In this particular case, d is the initial state quark and u has the highest probability to be produced after an interaction with a W boson but c and t can also be produced if there is enough energy.

179

An elementary process of a neutral weak interaction is an emission of a Z boson off a fermion line (right top diagram in Fig. 3). An electron is shown here as an example however it could also be any lepton, antilepton, quark or antiquark. Diagrams with a Z boson are very similar to ones with a photon except a photon can only be radiated off a charged particle but a Z boson can also be radiated off a neutrino or antineutrino.

185

The bottom diagrams in Fig. 3 are gauge bosons coupling diagrams including self-coupling of a W boson, its interaction with a Z boson and its electromagnetic radiation of a photon. WWZ , $WW\gamma$, $WWZZ$, $WWZ\gamma$, $WW\gamma\gamma$ and $WWWW$ vertices are all possible in the SM.

189

Electromagnetic and weak interactions are unified by the electroweak Glashow-Weinberg-Salam (GWS) theory which is based on $SU(2) \times U(1)$ symmetry. $SU(2)$ is the symmetry of weak isospin which generates three bosons: W^1 , W^2 and W^3 . $U(1)$ is the symmetry of the weak hypercharge and generate one neutral boson B . W^1 and W^2 are mixed to create W^+ and W^- mediators while W^3 and B are mixed to create a Z boson and a photon. Therefore, the GWS theory considers electromagnetic and weak forces as different manifestations of the electroweak force.

196

However, weak interactions are mediated by heavy bosons ($M_W = 80$ GeV, $M_Z = 91$ GeV) while electromagnetic interactions are mediated by a massless photon, thus, the electroweak symmetry is broken. To explain this phenomenon, the Higgs mechanism was introduced. The mechanism predicted an existence of an additional boson: the Higgs boson. The Higgs boson was a missing piece of the SM for many years and was finally discovered in 2012 at LHC by ATLAS and CMS collaborations through the processes shown in Fig.4 [3], [4].

203

The measurement in this dissertation is an electroweak measurement because the process in-

204

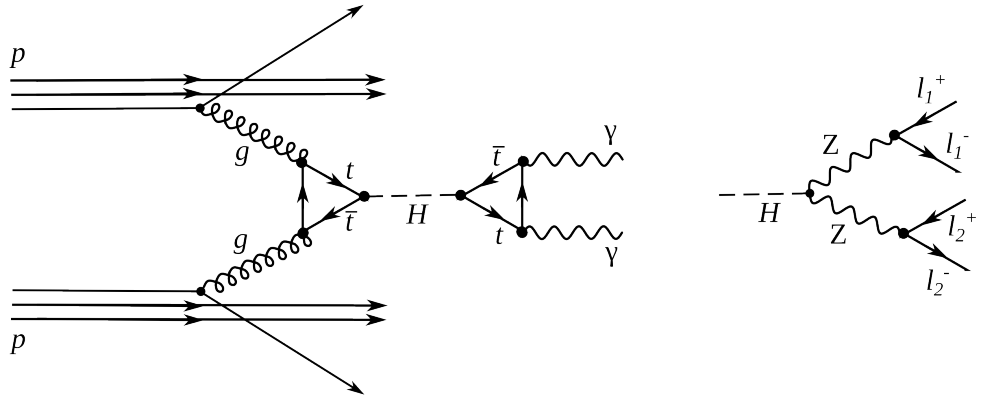
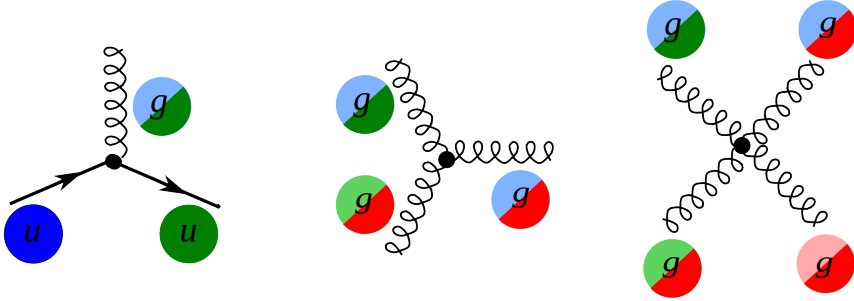


Figure 4: The Higgs boson production and decay

²⁰⁵ involves a W boson. It includes an interaction of a W boson with leptons and quarks as well as the
²⁰⁶ triple gauge coupling $WW\gamma$. Thus, the measurement is a good test of the SM electroweak theory.

²⁰⁷

208 **1.3 Strong Interactions**



213 Figure 5: Elementary processes of strong interactions

214 The third fundamental force after the electromagnetic and weak ones is the strong force. The
215 strong force is responsible for glueing protons and neutrons together in the nuclei as well as for
216 forming protons and neutrons themselves. The strong interactions occur by exchanging gluons
217 which are spin-one massless electrically neutral particles.

218 The elementary strong processes are shown in Fig. 5. There are three elementary processes:
219 qqg , ggg and $gggg$, all are involving particles with color charges. Thus, gluons couple to quarks
220 and self-couple. Color charges must be conserved at each elementary process of the strong in-
221 teraction. Because quarks can possess three colors, there are eight types of gluons to cover all
222 possible color exchanges.

223 The coupling constant of the strong interaction depends on a distance between interacting
224 particles: it becomes larger as the distance becomes larger. This property leads to two conse-
225 quences specific to the strong force: the confinement and the asymptotic freedom.

226 The asymptotic freedom means that when quarks are very close to each other they almost
227 do not interact with each other and therefore they are free. The confinement is the property
228 of quarks to always stay in the color neutral combinations (hadrons), it forbids the existence of
229 free quarks. A combination becomes color neutral when there is the same amount of color and
230 anticolor or if there is the same amount of each of the three colors. Thus, mesons are comprised
231 of a quark and an antiquark with the opposite color charges, and baryons are comprised of three
232 quarks: red, green and blue one. Examples of baryons include such well-known particles as a
233 proton and a neutron are baryons.

234 The strong interactions can be described by the QCD which is a quantum field theory in-
235 variant under $SU(3)$ color transformations. When the distance between quarks is small which
236 corresponds to high energy, and thus the coupling constant $\alpha_s \ll 1$ is small, the perturbative
237 approach can be used to compute observables.

238 The $W\gamma$ process being measured in this dissertation is not intended to test QCD, but a good
239 understanding of QCD is essential for performing this measurement because the QCD correc-
240 tions to the Feynman diagrams of the process are large and has to be taken into account in
241 producing simulation. Possible QCD corrections include quark-gluon loops at any of three quark
242 lines as well as exchanges of gluons between different quark lines. In addition, QCD describes
243 the dynamics of quarks and gluons within colliding protons and predicts probabilities of one or
244 another quark-antiquark pair to interact. Physics of proton-proton collisions is discussed in the
245 subsection 1.4.

247 1.4 Physics of Proton-Proton Collisions

248 At LHC two protons are collided. The LHC energy is so high that a proton behaves as a complex
 249 structure. A proton is a baryon, it consists of three quarks: uud . These three quarks are called
 250 valence quarks. They interact with each other by exchanging gluons which produce virtual $q\bar{q}$
 251 pairs (Fig. 6). Such quarks are called sea quarks.
 252

253 Any parton from one proton can interact with any parton from another proton. Probabilities
 254 $f_i(x, Q^2)$ of any particular constituent i to interact are described partially by QCD and par-
 255 tially by experimental measurements and depend on the momentum transfer Q and the momen-
 256 tum fraction of a specific parton x . These probabilities are called parton distribution functions
 257 (PDFs).
 258

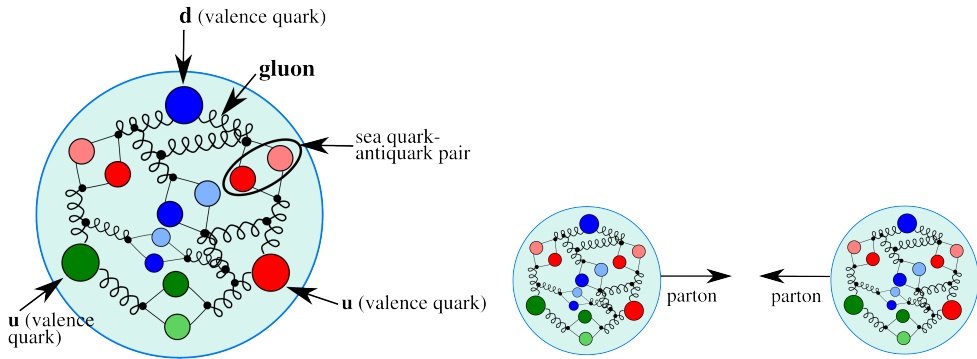


Figure 6: The proton structure (left) and the proton-proton collision (right).

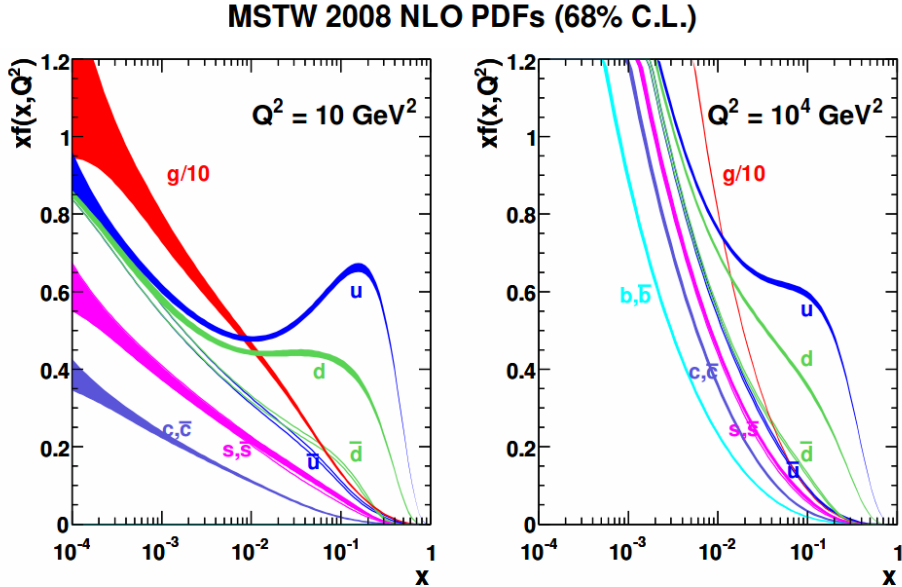


Figure 7: Martin-Stirling-Thorne-Watt parton distribution functions [5].

259 For large Q^2 and x gluon-gluon interactions have the largest probabilities to occur (Fig. 7).

260 However, gluons do not couple directly to a W boson, thus, in the $W\gamma$ measurement we are
261 mostly interested in quark-antiquark pairs which would have a total charge corresponding to the
262 charge of a W boson (± 1). Since we have u and d as valence quarks and we know that the
263 probability to couple to the same generation quark in charged weak interactions is the highest,
264 most of the W bosons are created by $u\bar{d}$ and $d\bar{u}$ pairs however other $q\bar{q}'$ combinations with the
265 total charges of ± 1 are also possible. The antiquarks come from virtual $q\bar{q}$ pairs inside of each
266 proton.

267
268 As we look for events containing $W\gamma$ we also have other events mimicking our process. Such
269 background events can be produced by any pair of partons.
270

271 1.5 Open Questions of the Standard Model

272 While the SM is an accurate description of all particle physics experimental results, there are
273 certain phenomena which are not included into the SM. In this subsection we discuss some of
274 them.

275 The gravitational interactions do not fit into the SM. It is the open question whether the
276 quantum theory of gravity is possible and whether there is a mediator of the gravitational in-
277 teractions. Also, it is not known why the gravitational force is so much weaker than any other
278 force. One possible explanation comes from a theory which predicts extra spatial dimensions
279 beyond the three we are dealing with (e.g. the string theory). In this case, it is possible that the
280 gravitational force is shared with other dimensions and that is why the fraction available in our
281 three dimensions is that small.

283 Another mystery of the Universe is its composition: it is known from the studies of the grav-
284 itational effects that our Universe consists of dark energy by 70%, of dark matter by 26% and of
285 baryon matter only by 4%. The dark energy resists the gravitational attraction and accelerates
286 the expansion of the Universe, and is not detectable by any effects except gravitational. The
287 understanding of the dark energy is a question of the general relativity rather than the particle
288 physics. The dark matter however likely consists of particles and therefore is a subject of the
289 particle physics. It does not radiate and that is why it cannot be detected by telescopes. The
290 nature of the dark matter is not known but its constituents must be very stable to remain since
291 the Big Bang. The theory of the supersymmetry which is unifying fundamental particles and
292 mediators predicts many of new heavy particles and the lightest supersymmetric particle, the
293 neutralino, is a good candidate for the dark matter.

295 One more open question is the reason for the matter/antimatter asymmetry. The matter
296 and antimatter should have been created in the same amount at the moment of the Big Bang.
297 Then most of it has annihilated but because of asymmetry, there was more matter than anti-
298 matter which led to the state of the Universe we observe now. There is a phenomenon of
299 the CP-violation in weak interactions observed and described that predicts the asymmetry at
300 a certain level. However, the effect of the CP-violation is not large enough to account for the
301 observed amount of the matter and, therefore, the total matter/antimatter asymmetry remains
302 unexplained.

304 The measurement of the photon transverse momentum spectrum (P_T^γ) of the $W\gamma$ process has
305 a goal to both test the SM and search for the BSM physics. The low P_T^γ region is not expected to
306 be affected by any new physics and must agree well with the SM predictions while the high P_T^γ
307 region may indicate an existence of a new physics if there is an enhance over the SM predictions.
308 The enhance would be an indirect evidence of the BSM particles like supersymmetric particles,
309 additional gauge bosons or higher generation fermions. More theoretical details about the SM
310 descriprion of $W\gamma$ process as well as the possible BSM physics are given in the chapter 2.

³¹³ **2 W γ Production Theory and Former Experimental Re-**

³¹⁴ **sults**

315 2.1 Electroweak Theory of the Standard Model

316 To develop a quantum field theory, we start with the Lagrangian of free fermions. In order
317 to describe a system with a conservation of a physical quantity, the Lagrangian is required to
318 satisfy a local invariance with respect to a certain transformation. For instance, a conservation
319 of an electric charge requires a local invariance under $U(1)$ transformation for the QED La-
320 grangian [6]. The requirement of the local invariance introduces an interaction of a new vector
321 field (or several fields) with our free fermions. The new vector field is a mediator of an inter-
322 action conserving the physical quantity. To provide a full description for a new boson field, in
323 addition to the interaction term we introduce an invariant term for the kinetic energy of the bo-
324 son. Such approach allows us to derive the Lagrangian which is locally invariant with respect to
325 a certain gauge transformation and contains interacting fermions as well as interaction mediators.
326

327 The SM is a quantum field theory invariant under the local $SU(3)_C \times SU(2)_L \times U(1)_Y$ trans-
328 formation [6]. The SM Lagrangian includes all observed quantum fields and their interactions.
329

330 The part of the SM Lagrangian based on the $SU(3)_C$ symmetry and is called QCD or theory
331 of strong interactions. QCD has three types of charges which are called colors: red, blue, and
332 green. To be a subject of strong interaction, a fermion must posses a color charge. Quarks
333 and antiquarks are such fermions. The requirement to satisfy the gauge invariance with respect
334 to $SU(3)_C$ transformations generates eight massless gluons, and the non-abelian nature of the
335 $SU(3)$ group generates self-interactions of gluons including three-gluon and four-gluon vertices.
336

337 The part of the SM Lagrangian based on the $SU(2)_L \times U(1)_Y$ symmetry is a foundation of the
338 unified theory of electroweak interactions. $SU(2)_L$ reflects transformations in the weak isospin
339 space of left-handed fermions ([1], Ch. 9) while $U(1)_Y$ reflects transformations in a weak hyper-
340 charge space of all fermions. The requirement of the local gauge invariant generates four massless
341 vector bosons which are mediators of electromagnetic and weak interactions. The non-abelian
342 structure of $SU(2)$ group generates gauge boson couplings the same way as self-interactions of
343 gluons appear in QCD.

344 Mass terms for the vector bosons would violate the gauge invariance of the electroweak La-
345 grangian, however it is experimentally known that mediators of weak interactions are heavy
346 particles with masses $M_W = 80$ GeV and $M_Z = 91$ GeV. A possible solution of the discrepancy
347 is a mechanism of the spontaneous symmetry breaking. QED symmetry group $U(1)$ remains
348 unbroken because a photon is massless.
349

350 The mechanism of the Spontaneous Symmetry Breaking and the appearance of the mass
351 terms for W and Z boson is realized by introducing an additional doublet of scalar fields. After
352 that, the Lagrangian is being transformed in such a way that W and Z bosons acquire masses
353 through their interactions with a new particle: a Higgs boson (H). A photon does not couple to
354 the Higgs boson remaining a massless particle and keeping $U(1)_{QED}$ symmetry unbroken.
355

356 The measurement in this dissertation provides a test for the electroweak sector of the SM. We
357 will retrace the steps of the derivation of the EWK part of the SM Lagrangian starting from terms
358 of free fermions. The resulting Lagrangian accommodates electroweak gauge bosons including
359 their self-couplings. One of these self-couplings, $WW\gamma$, is the primary focus of our measurement.
360

361 It is experimentally known that dynamics of weak interactions depends on particle's chirality
362 ([1], Ch. 4.4.1). In particular, a W boson couples to left-handed fermions and right-handed an-
363 tifermions only. A Z boson couples to both left-handed and right-handed charged fermions and
364 antifermions but only to left-handed neutrinos and right-handed antineutrinos. Given different
365 properties of left-handed and right-handed fermions, they are treated differently by the elec-
366 troweak theory. $SU(2)$ doublets are introduced for the wave functions of left-handed fermions
367 while $SU(2)$ singlets are introduced for the wave functions of right-handed fermions. Equa-
368 tions 1 and 2 show wave functions for the first generation fermions. Wave functions for the other
369

³⁷⁰ two generations are constructed the same way.

³⁷¹

$$\psi_1(x) = \begin{pmatrix} u \\ d' \end{pmatrix}_L, \psi_2(x) = u_R, \psi_3(x) = d'_R. \quad (1)$$

$$\psi_1(x) = \begin{pmatrix} \nu_e \\ e^- \end{pmatrix}_L, \psi_2(x) = \nu_{eR}, \psi_3(x) = e^-_R. \quad (2)$$

³⁷² The state d' in Eq. 1 is a mixture of d , c and b quark's wave functions and is determined by the
³⁷³ quark mixing matrix which is also called Cabibbo-Kobayashi-Maskawa matrix [6]:

³⁷⁴

$$\begin{pmatrix} d' \\ c' \\ b' \end{pmatrix} = V \begin{pmatrix} d \\ c \\ b \end{pmatrix} \quad (3)$$

³⁷⁵ To derive the unified electroweak Lagrangian, we start with the free fermion terms:

³⁷⁶

$$L_0 = \sum_{j=1}^3 i\bar{\psi}_j(x)\gamma^\mu\partial_\mu\psi_j(x), \quad (4)$$

³⁷⁷ where γ^μ are Dirac matrices ([1], Ch. 7.1) and $\psi_j(x)$ are wave functions determined by Eqs. 1 and 2.

³⁷⁸

³⁷⁹ The wave function ψ_1 changes under the $SU(2)_L \times U(1)_Y$ transformations in the following
³⁸⁰ way:

³⁸¹

$$\psi_1(x) \rightarrow e^{iy_1\beta}U_L\psi_1(x), \quad (5)$$

³⁸² while the wave functions $\psi_{(2,3)}(x)$ are singlets of $SU(2)_L$ and are affected only by $U(1)$ transfor-
³⁸³ mations:

³⁸⁴

$$eq : psi23_{transform}\psi_{(2,3)}(x) \rightarrow e^{iy_{(2,3)}\beta}\psi_{(2,3)}(x). \quad (6)$$

³⁸⁵ The transformation in the weak isospin space is defined as $U_L \equiv e^{i\sigma_i\alpha_i/2}$ where σ_i are Pauli
³⁸⁶ matrices ([1], Ch. 4.2.2). Phases $\alpha_i(x)$ and $\beta(x)$ in Eqs. 5 and ?? are arbitrary functions of x ,
³⁸⁷ and $y_{(1,2,3)}$ are weak hypercharges which are named analogous to electric charges in QED.

³⁸⁸

³⁸⁹ In order to satisfy the local $SU(2)_L \times U(1)_Y$ invariance, partial derivatives in Eq. 4 have to
³⁹⁰ be substituted with covariant derivatives:

³⁹¹

$$D_\mu\psi_1(x) = [\partial_\mu - ig\tilde{W}_\mu(x) - ig'y_1B_\mu(x)]\psi_1(x) \quad (7)$$

$$D_\mu\psi_{(2,3)}(x) = [\partial_\mu - ig'y_{(2,3)}B_\mu(x)]\psi_{(2,3)}(x) \quad (8)$$

³⁹² where g , g' are arbitrary constants,

³⁹³

$$\tilde{W}_\mu(x) \equiv \frac{\sigma_i}{2}W_\mu^i(x) = \frac{1}{\sqrt{2}} \begin{pmatrix} \sqrt{2}W_\mu^3 & (W_\mu^1 - iW_\mu^2)/\sqrt{2} \\ ((W_\mu^1 + iW_\mu^2)/\sqrt{2} & -W_\mu^3 \end{pmatrix}, \quad (9)$$

³⁹⁴ B_μ , W_μ^1 , W_μ^2 , W_μ^3 are four vector bosons that arise from the requirement of the Lagrangian to
³⁹⁵ be invariant under local $SU(2)_L \times U(1)$ transformations.

³⁹⁶

397 The Lagrangian becomes:

398

$$L_0 \rightarrow L = \sum_{j=1}^3 i\bar{\psi}_j(x)\gamma^\mu D_\mu \psi_j(x) \quad (10)$$

399 To make new vector bosons physical fields it is necessary to add terms for their kinetic energies:

400

$$L_{KIN} = -\frac{1}{4}B_{\mu\nu}B^{\mu\nu} - \frac{1}{4}W_{\mu\nu}^i W_i^{\mu\nu} \quad (11)$$

401 where $B_{\mu\nu} \equiv \partial_\mu B_\nu - \partial_\nu B_\mu$, $W_{\mu\nu}^i \equiv \partial_\mu W_\nu^i - \partial_\nu W_\mu^i + g\epsilon^{ijk}W_\mu^j W_\nu^k$

402

403 Off-diagonal terms of \tilde{W}_μ are wave functions of charged vector bosons $W^\pm = (W_\mu^1 \mp iW_\mu^2)/\sqrt{2}$
404 while W_μ^3 and B_μ are neutral fields which are mixtures of a Z boson and a photon determined by:

405

$$\begin{pmatrix} W_\mu^3 \\ B_\mu \end{pmatrix} \equiv \begin{pmatrix} \cos\theta_W & \sin\theta_W \\ -\sin\theta_W & \cos\theta_W \end{pmatrix} \begin{pmatrix} Z_\mu \\ A_\mu \end{pmatrix} \quad (12)$$

406 where θ_W is an electroweak mixing angle, A_μ is a photon field.

407

408 In order to be consistent with QED, terms involving A_μ in the electroweak Lagrangian must
409 be equal to the corresponding terms in QED Lagrangian [6]:

410

$$L_{QED} = i\bar{\psi}(x)\gamma^\mu \partial_\mu \psi(x) - m\bar{\psi}(x)\psi(x) + qA_\mu(x)\bar{\psi}(x)\gamma^\mu \psi(x) - \frac{1}{4}F_{\mu\nu}(x)F^{\mu\nu}(x), \quad (13)$$

411 where q is electric charge of $\psi(x)$ field, $F_{\mu\nu} \equiv \partial_\mu A_\nu - \partial_\nu A_\mu$.

412

413 This requirement relates g , g' , θ_W and e as $g \sin\theta_W = g' \cos\theta_W = e$ and provides expression
414 for weak hypercharges: $y = q - t_3$, where q is the electric charge and t_3 is a z -component of the
415 weak isospin. This results in $y_1 = 1/6$, $y_2 = 2/3$, and $y_3 = -1/3$ for quarks and $y_1 = -1/2$,
416 $y_2 = 0$, and $y_3 = -1$ for leptons. A right-handed neutrino has a weak hypercharge of $y_2 = 0$. It
417 also does not have an electric charge and, as a right-handed fermion, has $t_3 = 0$ and, therefore,
418 does not couple to a W boson. Thus, a right-handed neutrino does not participate in any SM
419 interaction.

420

421 Writing \tilde{W}_μ in Eq. 11 explicitly, we obtain TGC and QGC coupling terms:

422

$$L_{TGC} = -\frac{g}{4}(\partial_\mu W_\nu^i - \partial_\nu W_\mu^i)\epsilon^{ijk}W^{\mu j}W^{\nu k} - \frac{g}{4}\epsilon^{ijk}W_\mu^j W_\nu^k(\partial^\mu W^{\nu i} - \partial^\nu W^{\mu i}) \quad (14)$$

$$L_{QGC} = -\frac{g^2}{4}\epsilon^{ijk}\epsilon^{ilm}W_\mu^j W_\nu^k W^{\mu l}W^{\nu m} \quad (15)$$

423

Substituting W_μ^i and B_μ in Eq. 14 and Eq. 15 with the wave functions of W^\pm , Z and a photon:

424

$$B_\mu = -\sin\theta_W Z_\mu + \cos\theta_W A_\mu, \quad W_\mu^3 = \cos\theta_W Z_\mu + \sin\theta_W A_\mu, \quad (16)$$

$$W_\mu^1 = \sqrt{2}(W^+ + W^-), \quad W_\mu^2 = \sqrt{2}(W^- + W^+), \quad (17)$$

425

we receive charged TGC and QGC Lagrangians in the forms of Eqs. 18 and 21.

426

427

Equation 18 involves WWZ (Eq. 19) and $WW\gamma$ (Eq. 20) interactions:

428

$$L_{TGC} = L_{TGC}^{(1)} + L_{TGC}^{(2)}, \quad (18)$$

$$L_{TGC}^{(1)} = -ie \cot \theta_W (W^{-\mu\nu} W_\mu^+ Z_\nu - W^{+\mu\nu} W_\mu^- Z_\nu + W_\mu^- W_\nu^+ Z^{\mu\nu}), \quad (19)$$

$$L_{TGC}^{(2)} = -ie (W^{-\mu\nu} W_\mu^+ A_\nu - W^{+\mu\nu} W_\mu^- A_\nu + W_\mu^- W_\nu^+ A^{\mu\nu}). \quad (20)$$

429 Equation 21 involves $WWWW$ (Eq. 22), $WWZZ$ (Eq. 23), $WWZ\gamma$ (Eq. 24), and $WW\gamma\gamma$
430 (Eq. 25) interactions:

431

$$L_{QGC} = L_{QGC}^{(1)} + L_{QGC}^{(2)} + L_{QGC}^{(3)} + L_{QGC}^{(4)}, \quad (21)$$

$$L_{QGC}^{(1)} = -\frac{e^2}{2 \sin^2 \theta_W} (W_\mu^+ W^{-\mu} W_\nu^+ W^{-\nu} - W_\mu^+ W^{\mu} W_\nu^- W^{-\nu}), \quad (22)$$

$$L_{QGC}^{(2)} = -e^2 \cot^2 \theta_W (W_\mu^+ W^{-\mu} Z_\nu Z^\nu - W_\mu^+ Z^\mu W_\nu^- Z^\nu), \quad (23)$$

$$L_{QGC}^{(3)} = -e^2 \cot \theta_W (2W_\mu^+ W^{-\mu} Z_\nu A^\nu - W_\mu^+ Z^\mu W_\nu^- A^\nu - W_\mu^+ A^\mu W_\nu^- Z^\nu), \quad (24)$$

$$L_{QGC}^{(4)} = -e^2 (W_\mu^+ W^{-\mu} A_\nu A^\nu - W_\mu^+ A^\mu W_\nu^- A^\nu). \quad (25)$$

432 In the measurement of this dissertation we probe $WW\gamma$ coupling (Eq. ??).

433

434 The unified electroweak Lagrangian discussed above involves kinetic energy terms for fermions
435 and gauge bosons as well as interactions of fermions with gauge bosons, TGC, and QGC. How-
436 ever, this Lagrangian does not contain any mass terms. Because left-handed and right-handed
437 wave functions transform differently under the electroweak symmetry, adding fermion mass terms
438 of $\frac{1}{2}m_f^2 \bar{\psi}\psi$ would violate the Lagrangian invariance and, therefore, fermion mass terms are for-
439 bidden by the $SU(2) \times U(1)$ symmetry requirement. Mass terms for gauge bosons also would
440 violate the Lagrangian invariance just as a photon mass term $\frac{1}{2}m^2 A^\mu A_\mu$ would violate $U(1)$
441 invariance of L_{QED} [1]. Therefore, Lagrangian L in Eq. 10 contains massless particles only.

442

443 However, it is known from experiments that a Z boson, a W boson and fermions are massive
444 particles and, therefore, our theory should accommodate their masses. To introduce masses into
445 the electroweak Lagrangian, an $SU(2)_L$ doublet of complex scalar fields $\phi(x)$ is added to the
446 Lagrangian:

447

$$\phi(x) \equiv \begin{pmatrix} \phi^{(+)}(x) \\ \phi^{(0)}(x) \end{pmatrix} \quad (26)$$

448 By selecting a special gauge of $\phi(x)$ it is possible to spontaneously break electroweak sym-
449 metry, generate a new scalar particle, a Higgs boson [6], and introduce mass terms for W and
450 Z bosons and charged fermions through their couplings to the Higgs boson. The strength of the
451 coupling constant is proportional to the square of the particle's mass, therefore, heavier particles
452 are more likely to interact with H , and massless particles do not couple to H .

453

454 The mechanism of generating a fermion's mass involves both left-handed and right-handed
455 components of the fermion. If our hypothesis that right-handed neutrinos do not exist is right,
456 then the Higgs mechanism does not generate neutrino masses. However, from the experiments
457 of neutrino oscillations, neutrinos are known to have masses even though they are orders of
458 magnitude smaller than those of other fermions. Several hypotheses were offered to resolve this
459 contradiction however at the moment the mechanism of neutrinos to acquire masses remain un-
460 known [7].

461

462 In this dissertation, we study an electroweak process $W\gamma \rightarrow l\nu_l\gamma$, more specifically, probe
463 TGC vertex $WW\gamma$ (Eq. 20). To do that, we are measuring a differential cross section with
464 respect to the photon transverse momentum. The concept of the cross section in particle physics
465 is discussed in the next chapter.

466

2.2 Cross Section and Luminosity

In this dissertation we are measuring the total and the differential cross section. The cross section in particle physics is the interaction probability per unit flux of incident particles [12]. It can be interpreted as area which must be crossed by an incident particle in order to interact with a scattering center, or, in case of a differential cross section, area $d\sigma$ within which an incident particle must appear to be scattered off by an angle $d\theta$ (Fig. 8). The relationship between $d\sigma$ and $d\theta$ gives us the expression for a differential cross section $d\sigma/d\theta$. Integrating over $d\theta$, one would get the total cross section σ .

In Fig. 8 an incident particle is the same as a final state particle, however in particle physics final state particles can differ from initial state particles, and we measure a differential cross section with respect to a parameter X of the final state particle. Differentiating σ by X we get the expression for the differential cross section $d\sigma/dX$.

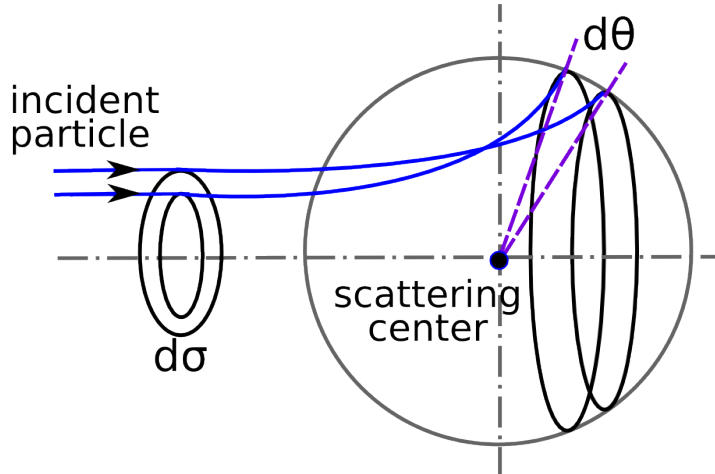


Figure 8: Illustration of the differential cross section concept in the classical case.

Referring to the Fig. 8, a number of particles passing through the area σ per unit time is $N = L \cdot \sigma$, where L is the flux of incident particles and is called luminosity. Therefore, the cross section σ of a specific process can be determined from an experiment as $\sigma = N/L$.

A cross section also can be computed theoretically. The formula to compute a cross section is:

$$\sigma = \frac{W_{fi}}{L} N_{fs}, \quad (27)$$

where W_{fi} is a transition probability between final and initial states of the system per unit volume, L is the flux of initial particles, and N_{fs} is the density of final states [8], Ch. 4.3.

The formula of the cross section is called the Fermi's Golden Rule [1]. In case of the scattering of two particles to three final state particles $1 + 2 \rightarrow 3 + 4 + 5$, it takes the following form:

$$\sigma = \frac{1}{4\sqrt{(p_1 p_2)^2 - (m_1 m_2)^2}} \int |M|^2 (2\pi)^4 \delta^4(p_1 + p_2 - p_3 - p_4 - p_5) \prod_{j=3}^5 \frac{1}{2\sqrt{\bar{p}_j^2 + m_j^2}} \frac{d^3 \bar{p}_j}{(2\pi)^3}, \quad (28)$$

493 where p_i are 4-momenta and \bar{p}_i are three momenta of the initial state and the final state
494 particles, m_i are masses of particles, M is the process amplitude determined by the dynamics
495 of the particles interaction. All available momenta of the final state particles is called the phase
496 space.

497

498 The cross section of the hard scattering in proton-proton collisions $pp \rightarrow X + Y$ has two
499 ingridients: PDFs and a partonic cross section $\sigma_{ab \rightarrow X}$. The partonic cross section is described
500 by perturbative QCD while PDFs require non-perturbative computations and are determined,
501 in part, from experiments (Fig. 7). According to the QCD factorization theorem [9]:

502

$$\sigma(pp \rightarrow X + Y) = \sum_{a,b} \int dx_a dx_b f_a(x_a, Q^2) f_b(x_b, Q^2) \sigma(ab \rightarrow X). \quad (29)$$

503 In case of $W\gamma$ process, X is $l\nu\gamma$, ab are $q_i\bar{q}_j$ or $q_j\bar{q}_i$. Q^2 is the large momentum scale that char-
504 acterizes hard scattering, f_a and f_b are PDFs, x_a and x_b are fractions of momenta of the partons.

505

2.3 Standard Model $W\gamma$ Production

A W boson in proton-proton collisions can be produced in the processes $q\bar{q}' \rightarrow W$ where q and \bar{q}' are a quark and an antiquark which have a total charge of +1 if producing a W^+ boson or of -1 if producing a W^- boson. The processes $u\bar{d} \rightarrow W^+$ and $d\bar{u} \rightarrow W^-$ are the most likely to occur because u and d are valence quarks in a proton. Antiquarks \bar{d} and \bar{u} come from sea $q\bar{q}$ pairs of the other proton.

A W boson decays immediately after being created, and we do not detect the W boson itself but its decay products. Decay modes of a W boson include $W^\pm \rightarrow l^\pm \nu_l (\bar{\nu}_l)$ where $l^\pm = e^\pm, \mu^\pm$ or τ^\pm with branching fractions of 11% per a leptonic channel [7]. The rest 67% stands for various $W \rightarrow q\bar{q}'$ decays. In this dissertation we only consider $W^\pm \rightarrow \mu^\pm \nu_\mu (\bar{\nu}_\mu)$ and $W^\pm \rightarrow e^\pm \nu_e (\bar{\nu}_e)$ as the cleanest channels.

A photon can be emitted from any charged particle of the process: a quark, an antiquark, a charged lepton or a W boson (Fig. 9, top). A quark and an antiquark are initial state particles and, therefore, if one of them radiates a photon, we call such process the Initial State Radiation (ISR). A muon or an electron is a final state particle and if it radiates a photon, we call such process the Final State Radiation (FSR). Finally, a W boson is a gauge boson and if it radiates a photon, the process has a vertex with three gauge bosons: $WW\gamma$, and we call such process the Triple Gauge Coupling (TGC).

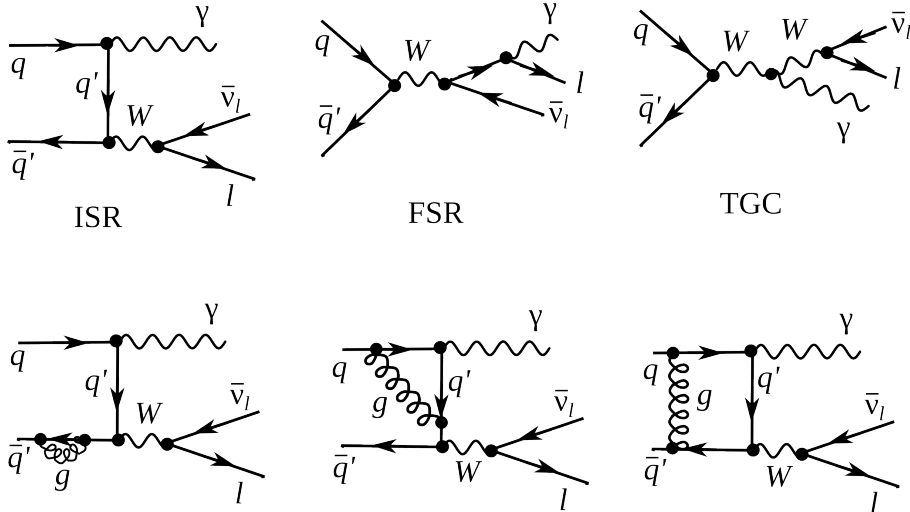


Figure 9: Feynman diagrams of $W\gamma$ production

The electroweak Lagrangian is described in Chapter 2.1. It is possible to derive equations of motion from the Lagrangian for any fields involved [1]. However, in a quantum field theory equations of motion cannot be solved exactly and, therefore, the perturbative approach is used if coupling constants are $g \ll 1$.

To represent the process graphically Feynman diagrams were invented. Also the diagrams can be used to calculate the process amplitude M from Eq. 28 because they are determined by Lagrangian terms relevant to the process. There is infinite number of Feynman diagrams corresponding to any specific process and the total amplitude of the process is a sum of individual amplitudes of each diagram and it is not technically possible to take into account all of them.

537 The perturbative approach arranges all the diagrams by orders of contribution because each
538 vertex is assigned a coupling constant and, therefore, the Feynman diagrams with fewer vertices
539 would give a significantly larger contribution to the amplitude. In Fig. 9 we have examples of the
540 Leading Order (LO) and the Next-to-Leading Order (NLO) Feynman diagrams (top and bottom
541 diagrams respectively).

542

543 The $W\gamma$ process is represented by four LO Feynman diagrams with three vertices each. The
544 $W\gamma$ process amplitude and cross section are long, complicated expressions, therefore, they are not
545 quoted in this dissertation. The first calculation of the $W\gamma$ process with necessary formulas can
546 be found in [14].

547

548 The NLO corrections shown in Fig. 9 are QCD corrections only which include gluon loops
549 at the same quark line and exchange of a gluon between two different quark lines however QED
550 and weak NLO diagrams are also possible. QED corrections mean radiations of extra photons
551 by charged particles, exchange of photons between different charged particles or a photon can be
552 radiated and absorbed by the same charged particle forming a loop. Similarly, weak corrections
553 mean extra virtual W or Z bosons. But the QCD corrections are the largest.

554

555 The theoretical cross section in particle physics is important not only for analyzing the mea-
556 surement result but also for producing the simulation which is then actively used while performing
557 the measurement. The simulation consists of two parts: the generation of the process and the
558 simulation of the particles paths through the detector. While the second one depends on the
559 well-known properties of the particles and the detector configurations, the first part relies on the
560 theory.

561

562 The most precise theoretical $W\gamma$ cross section available is the Next-to-Next-to-Leading Order
563 (NNLO) cross section in QCD [15]. The effect of the NNLO correction ranges from 19% to 26%
564 compared to the NLO cross section depending on the selection conditions. The contributions
565 from the higher order corrections is estimated to be $\pm 4\%$. However, the NNLO theoretical result
566 was published in 2015 only and there is still no simulation available based on that result. The
567 simulation used in this analysis is LO + up to two hadronic jets simulation which found to give
568 the same predictions as the NLO result.

569

570 In addition to the SM predictions, there are certain BSM theories which predict an enhance-
571 ment of the contribution from the TGC diagram. The discussion of these BSM effects and how
572 they affect the $W\gamma$ process takes place in Chapter 2.4.

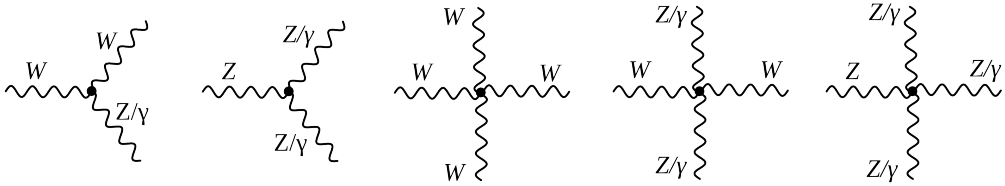
573

574 2.4 Anomalous $W\gamma$ Production

575 Most BSM physics theories predict the existence of particles which are heavier than the discov-
 576 ered energy range. If their masses are not accessible even by the most energetic machines, the
 577 direct detection of such particles is not possible. However, they can contribute to the productions
 578 of lower energetic particles producing loops where such heavy particles would be off-shell. The
 579 loops would give additional contributions to the process amplitude and, therefore, there would
 580 be more events produced in the process than one can expect based on the SM predictions.

581 These effects can be probed by precision measurements of the SM processes. In the elec-
 582 troweak sector processes of such interest include diboson and triboson productions which can
 583 occur through triple gauge couplings and quartic gauge couplings.

584 Triple and quartic gauge couplings (QGC) are represented by vertices with three and four
 585 bosons (Fig. 10). As discussed in Chapter 2.1, charged TGC and QGC are possible at tree level
 586 in the SM while neutral TGC and QGC are not.



589 Figure 10: TGC and QGC vertices

590 To account for the effects from the potential loops of heavy particles, we introduce an ef-
 591 fective Lagrangian with arbitrary values of coupling constants which can be shrunk to the SM
 592 Lagrangian if these constants would have their SM values. Such approach makes our searches
 593 model-independent because we do not specify which exactly particles form the loops but instead
 594 just check whether there is a deviation from the SM.

595 In $W\gamma$ measurement we can probe $WW\gamma$ vertex only. The most general Lorentz invariant
 596 Lagrangian of this vertex takes the following form [17]:

$$598 iL_{eff}^{WW\gamma} = iL_{eff(1)}^{WW\gamma} + iL_{eff(2)}^{WW\gamma} + iL_{eff(3)}^{WW\gamma} \quad (30)$$

$$iL_{eff(1)}^{WW\gamma} = e[g_1^\gamma A^\mu (W_{\mu\nu}^- W^{+\nu} - W_{\mu\nu}^+ W^{-\nu}) + \kappa_\gamma W_\mu^+ W_\nu^- A^{\mu\nu} + \frac{\lambda_\gamma}{m_W^2} A^{\mu\nu} W_\nu^{+\rho} W_{\rho\mu}^-] \quad (31)$$

$$iL_{eff(2)}^{WW\gamma} = e[i g_5^\gamma \epsilon_{\mu\nu\rho\sigma} ((\partial^\rho W^{-\mu}) W^{+\nu} - W^{-\mu} (\partial^\rho W^{+\nu})) V^\sigma + i g_4^\gamma W_\mu^- W_\nu^+ (\partial^\mu A^\nu + \partial^\nu A^\mu)] \quad (32)$$

$$iL_{eff(3)}^{WW\gamma} = e[\frac{\tilde{\kappa}_\gamma}{2} W_\mu^- W_\nu^+ \epsilon^{\mu\nu\rho\sigma} A_{\rho\sigma} - \frac{\tilde{\lambda}_\gamma}{2m_W^2} W_{\rho\mu}^- W_\nu^{+\mu} \epsilon^{\nu\rho\alpha\beta} A_{\alpha\beta}] \quad (33)$$

599 where e is the absolute value of the electron charge, A^μ is the photon field, $W^{\pm\mu}$ are fields of
 600 W^\pm bosons, $W_{\mu\nu} = \partial_\mu W_\nu - \partial_\nu W_\mu$, $A_{\mu\nu} = \partial_\mu A_\nu - \partial_\nu A_\mu$, m_W is the mass of a W boson, g_1^γ , κ_γ ,
 601 λ_γ , g_5^γ , g_4^γ , $\tilde{\kappa}_\gamma$, and $\tilde{\lambda}_\gamma$ are constants.

602

603 Despite there are 7 constants in the extended Lagrangian, only λ_γ and κ_γ are considered
 604 in the aTGC searches. The rest of the constants are fixed to their SM values based on various
 605 considerations. Thus, $g_1^\gamma = 1$ and $g_5^\gamma = 0$ are fixed to obey the electromagnetic gauge invariance
 606 for the on-shell photons. The non-zero value of g_5^γ also violates C and P conservations, and
 607 non-zero values of g_4^γ , κ_γ , $\tilde{\lambda}_\gamma$ violate the CP conservation law. Such violation parametrizations
 608 are not considered in charged TGC measurements now but might get considered in the future.
 609

610 The presence of aTGC would have larger effects at high energy scales. Fig. 11 shows these
 611 effect in P_T^γ spectrum of 7 TeV $W\gamma \rightarrow \mu\nu\gamma$ measurement. Fig. 12 shows the examples of these
 612 effects in m_{ll} spectrum in 8 TeV $WW \rightarrow l\nu l\nu$ measurement (left) and P_T^γ spectrum in 7 TeV
 613 $Z\gamma \rightarrow \nu\nu\gamma$ measurement (right). It is seen on the plots that aTGC spectrum at low m_{ll} or low
 614 P_T^γ coincides with the SM prediction but for higher m_{ll} or P_T^γ the disagreement becomes more
 615 significant.
 616

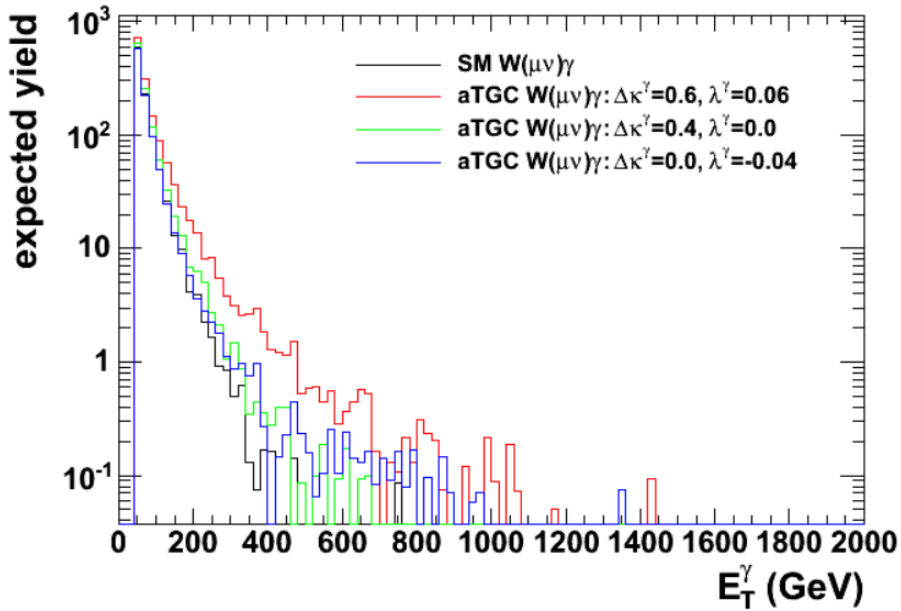


Figure 11: Distributions of P_T^γ of simulated $W\gamma \rightarrow \mu\nu\gamma$ events with different values of aTGC constants at LHC energy of $\sqrt{s} = 7$ TeV. Source of figure: [18].

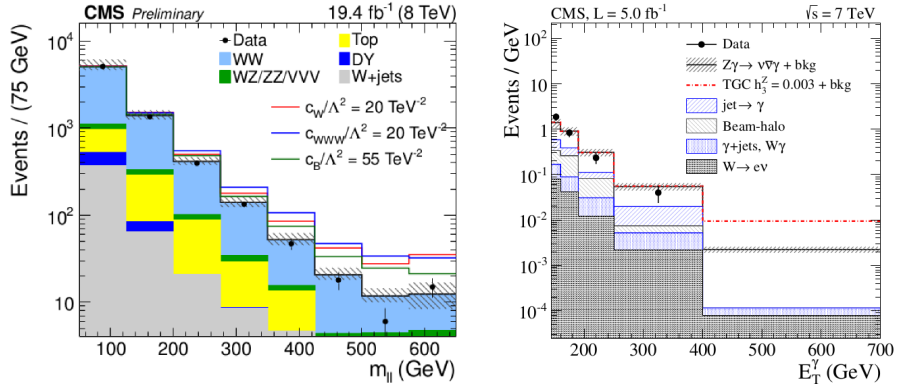


Figure 12: Examples of the potential effects of non-zero TGC constants in m_{ll} spectrum in 8 TeV $WW \rightarrow l\nu l\nu$ measurement (left) [29] and P_T^γ spectrum in 7 TeV $Z\gamma \rightarrow \nu\nu\gamma$ measurement (right) [30].

2.5 Measurements in the Past

ATGC parameters of $WW\gamma$ vertex can be probed in $W\gamma$, WW , and WZ measurements. Limits on $\Delta\kappa_\gamma$ and λ_γ constants from different D0 [19], LEP [20], ATLAS [21], [22], [23] and CMS [25], [26], [27], [28] measurements are summarized in Fig. 13.

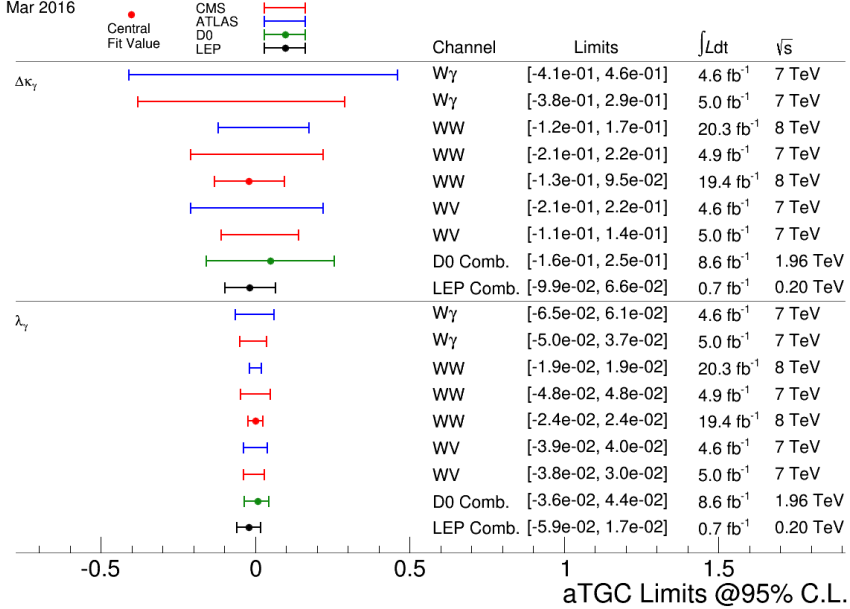


Figure 13: Summary of limits on the $WW\gamma$ aTGC coupling constants. Figure from [24]

The most recent measurements of $W\gamma$ production were performed by CMS [25] and ATLAS [21] collaborations with pp collisions at $\sqrt{s} = 7 \text{ GeV}$ collected in 2011. The measurements are based on 5 fb^{-1} and 4.6 fb^{-1} of integrated luminosity with CMS and ATLAS respectively. Both collaborations considered two channels: $W\gamma \rightarrow \mu\nu\gamma$ and $W\gamma \rightarrow e\nu\gamma$.

Dibosons processes are rare in pp -collisions and we have to filter out events of our interest from many processes which are more likely to happen. To do that, we apply variety of selection criteria which reject most of background events increasing our signal rate as much as possible. However, even after we applied all possible selection criteria, majority of our selected events are still background events and it is not possible to reduce the background any further without also significantly reducing signal.

The major source of such irreducible background is the fake photon background where hadronic jets are misidentified as photons. Such events originate from $W+\text{jets}$ process mostly but $Z+\text{jets}$ and $t\bar{t}+\text{jets}$ events contribute to this source of the background as well. The second major background for the electron channel is the fake photon background where electron can be misidentified as a photon. Such events are coming from $Z+\text{jets}$ events. Other sources of backgrounds include real- γ backgrounds, fake lepton + real photon and fake lepton + fake photon sources.

Both channels provide measurements of p_T^γ spectra because this variable is the most sensitive to the potential ATGC. The p_T^γ spectra of the selected events in data superimposed with selected events in the simulation of the signal and estimated background contribution for the muon and electron channels are shown in Fig. 14 for CMS and in Fig. 15 for ATLAS. Both measurements show a good agreement.

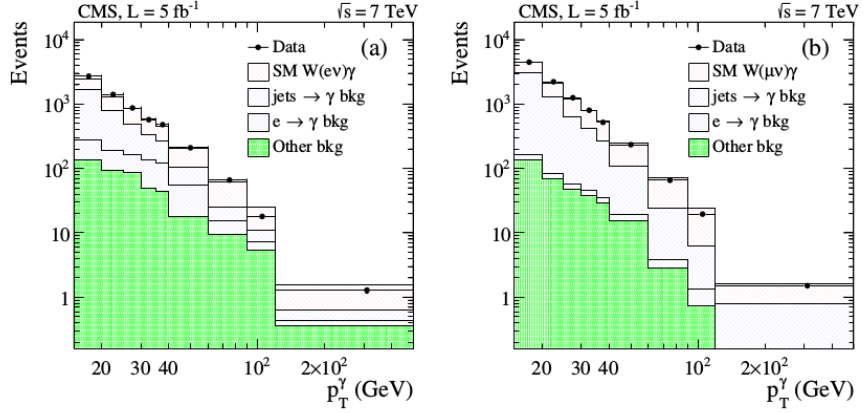


Figure 14: The distribution fo the p_T^γ of $W\gamma$ candidates in the analysis of 7 TeV CMS data. Data vs signal MC + background estimates. Left: $W\gamma \rightarrow e\nu\gamma$, right: $W\gamma \rightarrow \mu\nu\gamma$ [25].

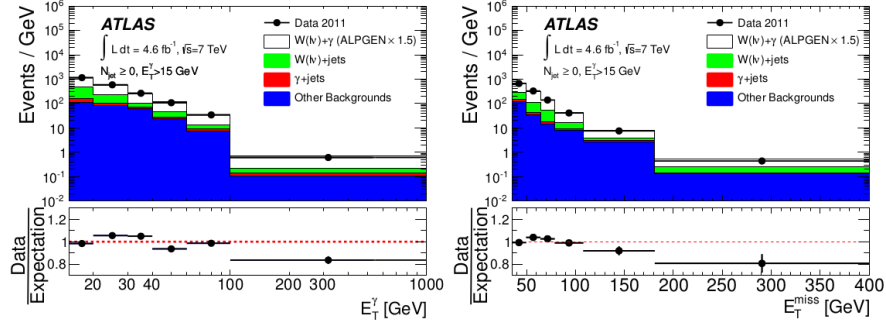


Figure 15: The distribution fo the p_T^γ (left) and E_T^γ (right) of $W\gamma$ candidates in the analysis of 7 TeV ATLAS data. Data vs signal MC + background estimates [21].

CMS provides measurements of the P_T^γ spectrum, the total cross section within the phase spaces of $\Delta R > 0.7$, $P_T^\gamma > 15$ GeV, $P_T^\gamma > 60$ GeV and $P_T^\gamma > 90$ GeV, and limits on aTGC coupling constants. The phase space restrictions come from the considerations of the detector acceptance, reducing heavily background-dominated regions and theory.

ATLAS, in addition to the P_T^γ spectrum, total cross section and limits, provides the differential cross section and cross section with different number of associated jets. No evidence of a new physics is observed.

In this dissertation we are measuring total and differential $d\sigma/dP_T^\gamma$ cross section however we do not derive limits on aTGC coupling constants. The measurement details and results are available in Chapter 5.

661 **3 Experimental Setup**

662 3.1 Large Hadron Collider

663 The Large Hadron Collider (LHC) [31], [32], [33] is the largest particle accelerator and the the
 664 most ambitious research facility ever built. LHC is placed into a tunnel originally built for the
 665 LEP accelerator. LEP was decommissioned to make room for LHC. The tunnel is about 27 km
 666 in circumference, located at the Swiss-French boundary up to 100 meters undergroud.

667 Before entering LHC, particle beams are going through several stages of the acceleration and
 668 LHC is the last element of the chain of the CERN's accelerator complex (Fig. 16). Protons are
 669 extracted from hydrogen atoms, are accelerated by Linac2 to energies of 5 MeV, then injected
 670 into the Proton Synchrotron Booster (PSB) where they reach energies of 1.4 GeV. After that
 671 protons are to PS and Super PS (SPS) where they are accelerated to 25 GeV and 450 GeV
 672 respectively. Finally, protons enter LHC and are accelerated for 20 minutes to reach their design
 673 energies of 7 TeV per beam. Besides protons, the complex also accelerates and collides lead ions
 674 however in this dissertation we analyze data from proton-proton collisions only and, therefore,
 675 are not discussing lead ion collisions.

676 Main goals of LHC were to detect the SM Higgs boson if it existed and to search for evidences
 677 of BSM physics which may give a clue on understanding the phenomena including but not limited
 678 to the dark matter, the matter-antimatter asymmetry, the nature of the gravitational force. Six
 679 detectors are installed at the LHC to detect particles and perform the relevant measurements.
 680 There are general purpose detectors ATLAS and CMS, there is LHCb which specializes of the
 681 physics of B-mesons, and ALICE which is designed to detect products of heavy ion collisions. In
 682 addition, there are two relatively small detectros: LHCf and TOTEM which are installed close
 683 to the ATLAS and CMS collision points respectively.

684 A new particle with mass $m = 125$ GeV was discovered by CMS [3] and ATLAS [4] collabora-
 685 tions in 2012. The particle is consistent with the SM Higgs boson predicted by the EWK sector
 686 of the SM. The discovery of the Higgs boson is the greatest achievement by the LHC to date.

687 No deviations from the SM were found by any of the experiments.

688 The design energy of LHC is 7 TeV per beam however several lower energy points were and
 689 are being probed. In 2010-2011 LHC operated at energy of 3.5 TeV per beam which was already
 690 higher than energy of any other collider. In 2012 the energy increased up to 4 GeV. In 2013-2014
 691 the LHC was shut down for upgrades. Collisions were restarted at 6.5 TeV in 2015 and the LHC
 692 is still operating at this energy in 2016.

693 All important measurements performed at lower energies are also repeated at higher energies
 694 because the ability to probe higher energy scales increases our chances for a discovery and even
 695 if no deviations from the known physics are found at a given energy point, the discovery is still
 696 possible to happen as we go higher in the energy.

697 In addition to the beam energy, one of the most important qualities of an accelerator is the
 698 ability to produce a large number of interesting collisions which is determined by the luminosity.
 699 The instantaneous luminosity is determined by the following expression [7]:

$$700 L = f \frac{n_1 n_2}{4\pi \sigma_x \sigma_y}$$

701 where n_1 and n_2 are numbers of particles in colliding bunches, f is a frequency of collisions,
 702 σ_x and σ_y are beam sizes in horizontal and vertical directions. To determine the integrated
 703 luminosity, one has to integrate the instantaneous luminosity over time:

$$704 L_{int} = \int L dt$$

705 The luminosity of the LHC is also higher than of any previously existed collider. The integrated
 706 luminosity of the LHC for different years of the operation are shown in Fig. 17. Run periods of

LHC in 2010-2012 refer to Run I of the LHC operation. While working on energy of $\sqrt{s} = 7$ TeV, LHC delivered 44.96 pb^{-1} and 6.1 fb^{-1} of data in 2010 and 2011 year respectively. In 2012 the working energy of LHC was $\sqrt{s} = 8$ TeV, and the integrated luminosity was $L_{int} = 23.3 \text{ fb}^{-1}$. After a long shutdown, LHC was upgraded for Run II, to operate on $\sqrt{s} = 13$ TeV in 2015 and delivered 4.22 fb^{-1} of data by the end of 2015. In 2016 LHC continues operation on $\sqrt{s} = 13$ TeV and by the end of September the integrated luminosity already exceeded a value of 30 fb^{-1} [37].

723

724

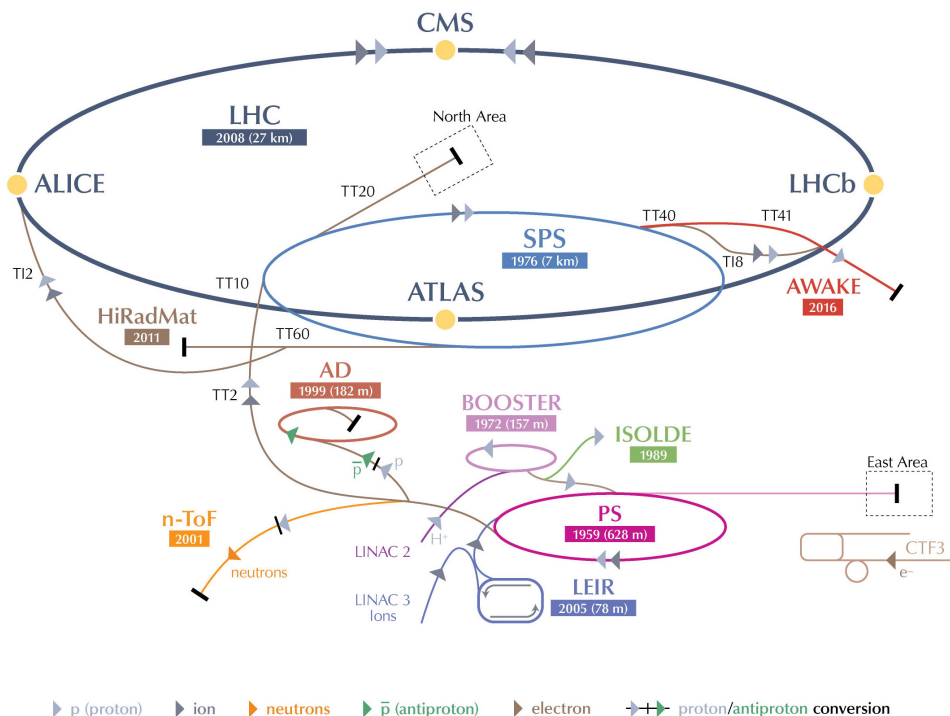
There are many other collider parameters which are not discussed in this dissertation. A brief summary of the most important of them is available in Tab. 2.

727

The measurement of this dissertation is performed at the energy of 4 TeV per beam or at the center of mass energy $\sqrt{s} = 8$ TeV using 19.6 fb^{-1} of data. Previous measurements of the same process were done at $\sqrt{s} = 7$ TeV with about four times less amount of data by both CMS and ATLAS. These measurements are discussed in greater details in Ch. 2.5.

732

CERN's Accelerator Complex



LHC Large Hadron Collider SPS Super Proton Synchrotron PS Proton Synchrotron

AD Antiproton Decelerator CTF3 Clic Test Facility AWAKE Advanced WAKEfield Experiment ISOLDE Isotope Separator OnLine Dvice

LEIR Low Energy Ion Ring LINAC LiNear ACcelerator n-ToF Neutrons Time Of Flight HiRadMat High-Radiation to Materials

© CERN2013

Figure 16: CERN's accelerator complex. Source of the figure: [34].

Table 2: Main parameters of LHC [31]

Circumference	27 km
Dipole operating temperature	1.9 K
Number of magnets	9593
Number of main dipoles	1232
Number of main quadrupoles	392
Number of RF cavities	8 per beam
Nominal energy, protons	7 TeV
Nominal energy, lead ions	2.76 TeV per nucleon
Peak magnetic dipole field	8.33 T
Min. distance between bunches	7 m
Design luminosity	$10^{34} \text{ cm}^{-2} \text{ s}^{-1}$
No. of bunches per proton beam	2808
No. of protons per bunch (at start)	1.1×10^{11}
No. of collisions per second	600 millions

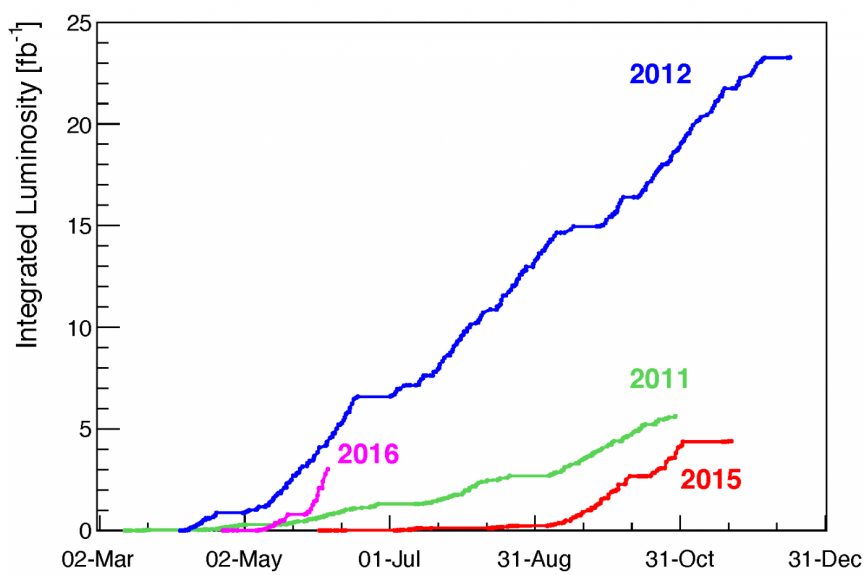


Figure 17: LHC integrated luminosity by year. Source of the figure: [35].

3.2 Compact Muon Solenoid

3.2.1 Introduction

CMS is a general-purpose detector designed for detecting various particles which are being produced in pp collisions at LHC. Its main feature is a huge magnet to create a magnetic field of 4T to curve charged particles in the tracking system and 2T outside to curve muons in the muon system.

CMS detector is a cylindrically symmetric with a colliding beam as a central axis. The detector consists, from inner to outer layer, of a tracking system, an electromagnetic calorimeter (ECal), a hadronic calorimeter (HCal), a magnet and a muon system. Having the tracking system, ECal and HCal inside of a large solenoid makes the detector "compact". A segment of a CMS slice in $r - \phi$ plane is shown in Fig. 18.

When a heavy particle is produced in a collision, it decays immediately, and we detect its long-living decay products including an electron, a photon, a muon, a neutral hadron or a charged hadron. Depending on the trace left by a particle in different subdetectors we can identify a particle. Electrons and positrons leave curved tracks in the tracking system and then induce showers in the electromagnetic calorimeter (ECal) where they are typically stopped. Photons induce the same electromagnetic showers in ECal however, as neutral particles, they do not leave tracks in the tracking system. Hadrons normally travel through the ECal undisturbed and induce a hadronic shower in the hadronic calorimeter (HCal). Charged and neutral hadrons can be distinguished from each other by checking whether they leave a track in the tracking system or not. Muons are the only particles which are not stopped by the layer of ferrum and leave tracks in the CMS muon system. Neutrinos are not detected by CMS.

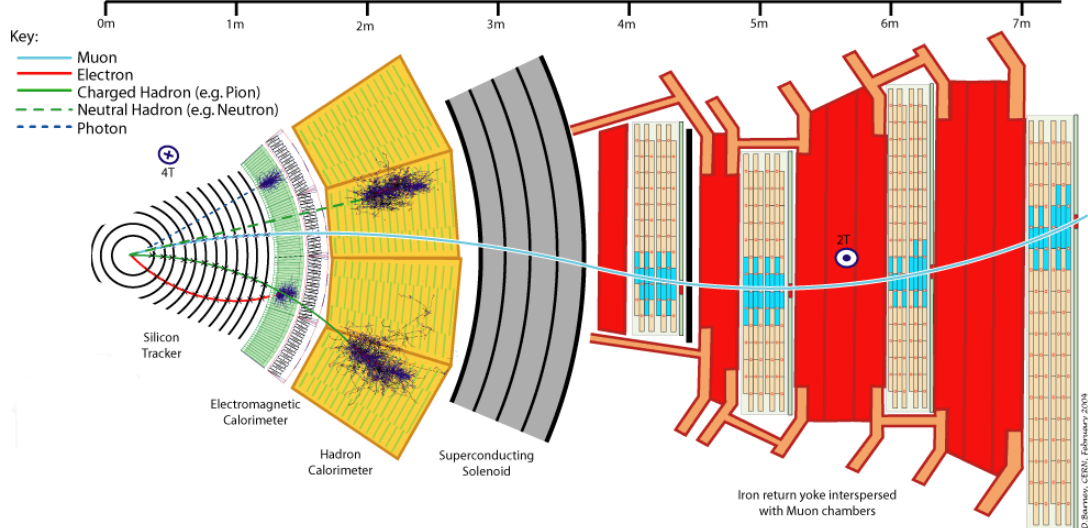


Figure 18: CMS slice.

In $W\gamma$ measurement we have muons and electrons as final state particles. They are both affected by CMS magnetic field allowing the tracking system and the muon system to measure their trajectory parameters and momenta.

In this dissertation we use the information of the primary vertex determined by the tracking system to select our events. Also the tracker provide us the information about electrons trajectories and momenta in the electron channel and distinguishes between electrons and photons.

764

765 **3.2.2 Magnet**

766 A magnetic field in a particle detector is necessary to measure momenta of charged particles
767 by track curvatures. The higher the momentum is, the less a particles's path is affected by the
768 magnetic field. In CMS it is done in the tracking system for all charged particles and in the
769 muon system for muons.

770

771 The CMS magnet is placed between layers of HCal and a muon system. It creates a magnetic
772 field of 4T inside the magnet, for the tracking system, and 2T outside the magnet, for the muon
773 system. It is necessary to have stronger field in the tracking system because a density of tracks
774 is much higher there than in the muon system and also the tracking system is much smaller and,
775 therefore, more significant curvature is necessary to measure the momentum with high precision.

776

777 The magnet is made of superconducting wires. An electric current flowing in the wires creates
778 a uniform field inside the solenoid and also provides a magnetic field of a certain configuration
779 outside the solenoid.

780

781 **3.2.3 Tracking System**

782 The tracking system measures track geometry including particles trajectories and locations of
783 primary and secondary vertices and momenta of charged particles. It needs to disturb particles
784 as little as possible so that they can pass through. Therefore, just a few measurements must be
785 enough to reconstruct the track. The accuracy of a measurement of each hit is $10 \mu\text{m}$.

786

787 The tracking system consists of silicon pixels and silicon strips (Fig. 19). Collision tracks
788 start at the center and then cross the layers of the tracking system. Tracks are straight in $r - z$
789 plane and curved by the magnetic field in the $r - \phi$ plane. The acceptance of the tracker sys-
790 tem in $r - z$ plane is geometrically limited by $\eta = 2.5$ ($\eta = -\ln[\tan \theta/2]$, where θ is a polar angle).

791

792 The pixel tracker is the closest subsystem of CMS to the collision point thus it receives the
793 largest particle flux: at 8 cm from the collision point the flux is about 10 million $1/(cm^2 s)$, and
794 the pixel detector with its 65 millions sensors is capable to reconstruct all these tracks. It consists
795 of three layers of cylinders in the barrel with radii of 4 cm, 7 cm and 11 cm and four disks in
796 the endcap, two disks at each side. The tracker is designed in such a way that a single track hits
797 multiple sensors. Then the trajectory is reconstructed based on how much charge is collected on
798 each sensor. This allows us to reach a spacial resolution of $15\text{-}20 \mu\text{m}$ which is much smaller than
799 a distance between sensors.

800

801 The strip tracker is placed right after the pixel tracker and occupies the detector volume up
802 to 130 cm around the beam axis. The strip tracker consists of four parts: the tracker inner barrel
803 (TIB), the tracker inner disks (TID), the tracker outer barrel (TOB) and the tracker endcap
804 (TEC) as shown in Fig. 19. In the strip tracker there are over 15,000 sensitive modules with a
805 total number of 10 million strips. Each sensitive module consists of a set of sensors, its support
806 structure and readout elements.

807

808 **3.2.4 Electromagnetic Calorimeter**

809 The ECal measures energy of electrons and photons and also measures geometries of their tra-
810 jectories. Electrons and photons interact with the ECal substance by inducing electromagnetic
811 showers. Traces left by photons and electrons in the ECal are the same. To distinguish between
812 these two particles, it is necessary to perform matching to the track in the tracking system. If

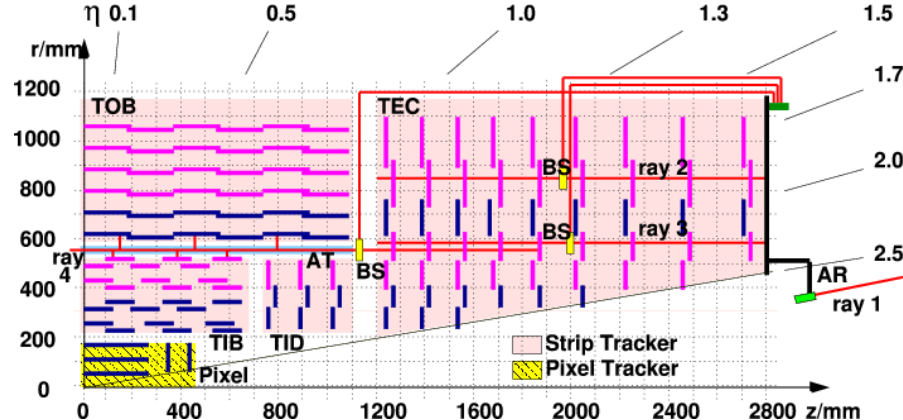


Figure 19: Slice of the CMS tracking system in $r - z$ plane.

813 there is a track, then there is an electron (or positron). If there is no track, then the particle is
 814 a photon.

815
 816 The Ecal is a layer between the tracking system and the HCal. It is made of high-density lead
 817 tungstate crystals arranged in a barrel section and two endcap sections. The crystals work as
 818 scintillators. When electrons and photons pass through it, it produces light proportional to the
 819 particle's energy. The scintillated light then is amplified by photomultipliers producing signals
 820 on sensitive elements.

821
 822 It is important for the Ecal to be able to distinguish between high energetic photons and
 823 pairs of lower energetic photons e.g. from a π^0 decay. It is especially difficult in the endcap
 824 sections where angle between two photon trajectories is small. Ecal preshower located in front
 825 of the endcaps which have much smaller granularity provide extra spacial precision. Their strips
 826 are 2 mm wide compared to 3 cm wide crystals in the main volume of the ECal.
 827

828 3.2.5 Hadron Calorimeter

829 The HCal is placed right after the ECal and is the last subdetector within the magnet. The
 830 HCal measures energies of charged and neutral hadrons. In addition, the HCal determines the
 831 track parameters. Match to the tracking system has to be done: if a matching track found, then
 832 it is a charged hadron otherwise it is a neutral hadron.

833
 834 The HCal consists of alternate layers of absorbers and scintillators. Hadrons hit brass or steel
 835 plate of absorber producing secondary particles. When emerge into the scintillator, the particles
 836 induce hadronic and electromagnetic showers and emit blue-violet light which is further shifted
 837 to the green region and read out by special boxes within the HCal. The secondary hadrons pro-
 838 duced during the interaction with the absorber interact with the next absorber producing more
 839 showers in the next layers of scintillators and also affect the total energy deposit. All hadrons
 840 must be stopped inside the layers of the HCal.
 841

842 3.2.6 Muon System

843 Muons pass through the ECal, the HCal and the magnet without interacting. They are the only
 844 particles which are registered in the muon system which is placed outside the magnet and which
 845 is the largest part of CMS detector.

846
847 There are four concentric layers of muon detectors (stations) and iron return yoke between
848 them. Muons induce several hits in the muon stations which are later fitted and matched to the
849 tracking system measurements to provide the best possible resolution in the measurements of all
850 parameters of the muon's trajectory and momentum.

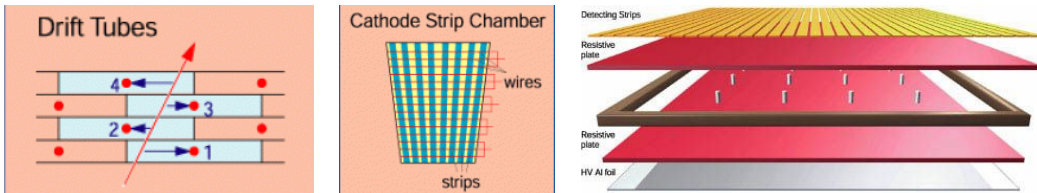
851
852 There are three types of muon chambers used in the CMS muon system: drift tubes (DTs),
853 cathode strip chambers (CSCs) and resistive plate chambers (RPCs). Overall, there are 1400
854 muon chambers including 250 DTs, 540 CSCs and 610 RPCs.

855
856 The system of DTs measures positions of muons in the barrel. Each DT chamber is about 2 m
857 by 2.5 m in size. It consists of 12 layers of aluminium which are grouped by four. There are up
858 to 60 drift tubes in a layer. The middle group of layers measures z -coordinate and two other
859 groups determine the perpendicular coordinate.

860
861 Each drift tube is 4 cm in width, is filled with a gas and has a wire inside. When a charged
862 particle passes through the volume, it ionizes atoms and the wire receives an electric charge.

863
864 CSCs are placed in endcap regions. CSCs are arrays of anode wires which are crossed by
865 copper cathode strips placed in a gas volume. When a charged particle penetrates to the gas
866 volume, it ionizes the gas. Electrons drift to the wires while ions move to the strips. Strips are
867 perpendicular to wires, thus, we measure two coordinates for each particle.

868
869 RPCs are parallel capacitors made of high-resistivity plastic plates with a space between
870 them filled with a gas. RPCs provide quick measurements of muon momenta and are used for
871 triggering.



872
873 Figure 20: Components of the CMS muon system. Left to right: drift tubes, cathode strip
chambers (CSCs), resistive plate chambers (RPCs).

873 3.2.7 Triggering and Data Aquisition

874 At peak luminosity, CMS experiences one billion proton-proton collisions per second which come
875 in bunches separated just by 25 ns from one other. New events come before the events from
876 the previous bunch crossing left the detector. To process the information from many different
877 collisions at the same time, data is stored in pipelines.

878
879 It is not technically possible to readout all these events. Moreover, we do not need most
880 of these events for a physics analysis because most of these events do not have a potential to
881 discover a new physics. We have resources to store about one hundred events out of one billion
882 that is why we need a trigger system which quickly decides what the best one hundred events are.

883
884 If the triggers were too loose, and we would select one hundred events too quickly, e.g., out
885 of a hundred million events, then CMS would not be able to process the rest 90% of events in a

givem set of one billion and we would lose 90% of potentially interesting events.

If the triggers were too strict, we would select, e.g., ten events out of one billion, not one hundred and lose CMS potential to store and process data by 90% which would significantly reduce our chances for a discovery.

Thus, the challenge of the trigger system is to select the best one hundred events out of one billion and do that fast to be able to process every single event. To achieve this goal, a two-level trigger system was developed consisting from the Level 1 (L1) trigger and the high level trigger (HLT) as shown in Fig. 21.

L1 is a hardware based trigger (Fig. 22). It uses information from the ECal, HCal and muon system. L1 reduces frequency of coming events from 40 MHz to 100 kHz. Events which did not pass the L1 trigger are lost forever while events which pass the L1 trigger are temporarily stored to get checked by the HLT.

HLT is a software-based trigger. It uses information from all subdetectors and runs quick reconstruction and identification algorithms to determine types of particles and their kinematics. It reduces the number of events to 100 Hz. Events which did not pass HLT are lost forever. Events which pass HLT are arranged into appropriate datasets depending on HLT selection criteria they passed and stored for physics analyses.

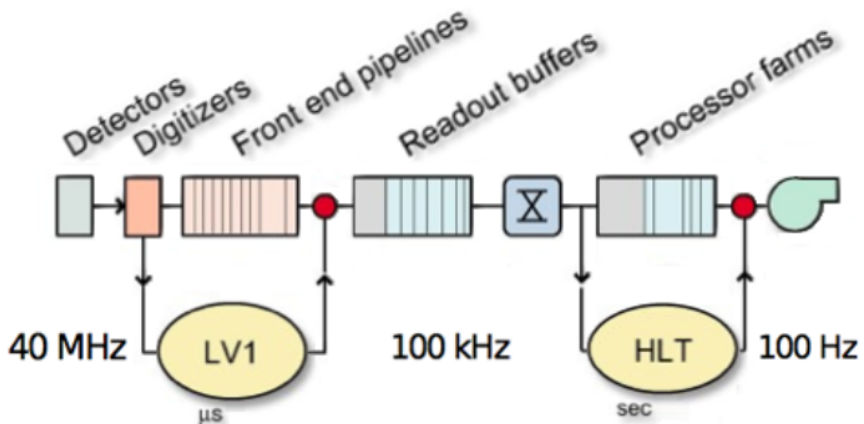


Figure 21: Two-level CMS trigger system.

3.2.8 Event Reconstruction

Where to place particle reconstruction, particle flow algorithm and MET? Check other theses
 Acceptance: particles which are too collinear and go to pipe; particles which get curved too strongly

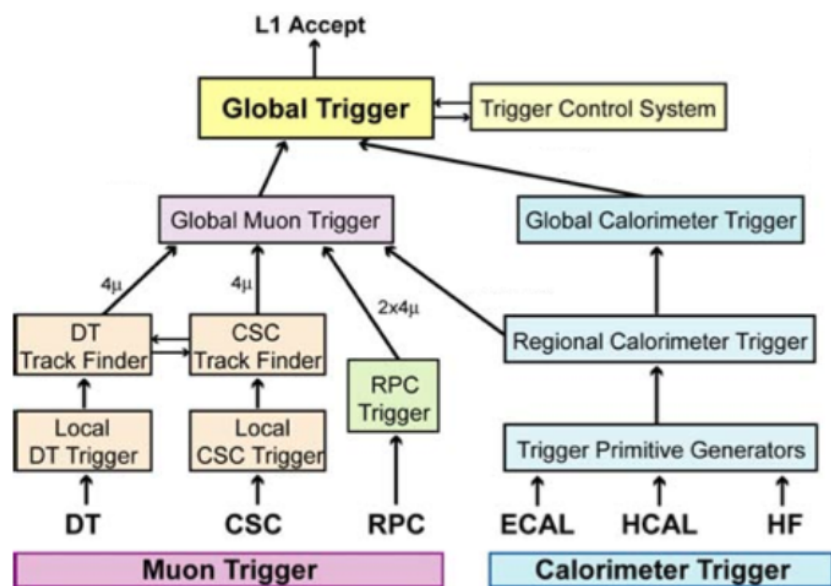


Figure 22: Level 1 CMS trigger system.

912 4 CMS Tracker Alignment

913 4.1 Algorithm

914 Why align?
 915 How to align?
 916 When align?
 917 How to check that your alignment is good?

918 A tracking system detects hits produced by a charged particle traveling through the detector.
 919 In a presence of a constant magnetic field the particle has a helical trajectory. A reconstruction
 920 algorithm determines the track parameters by fitting the positions of hits assuming the helix
 921 trajectory.

922 Better hit resolution and the location uncertainty lead to better precision of a measurement
 923 of the track parameters. The location uncertainty depends on our knowledge of the positions and
 924 orientations in space of the tracking system modules. The hit resolution in the CMS pixel detector
 925 is $\sim 15 \mu\text{m}$. When the modules are mounted, their positions are known with precision of $\sim 200 \mu\text{m}$.
 926 Thus, we need to know positions of modules 20 times better than they are known when mounted.

927 The procedure of the determination of the modules locations and orientations is called the
 928 tracker alignment. The concept of the track-based alignment can be illustrated in the example of
 929 the alignment of a toy tracker. When a charged particle passing through a detector (Fig. 23, top
 930 left) it crosses a toy tracker which consists of six flat equidistant modules (Fig. 23, top right). If
 931 the modules were placed exactly at their designed positions, we would observe the hits exactly at
 932 the points where the track crosses modules at the points of ideal geometry (Fig. 23, middle left).
 933 However, in a reality the positions and tilts of the modules are different from ones suggested by
 934 the ideal geometry (Fig. 23, middle right). Hits, indeed, are recorded at the places where mod-
 935 ules are actually mounted, not at the design ideal places (Fig. 23, bottom left). If we assumed a
 936 tracker to be ideal and a track to be smooth, we would see that our hits are off-track (Fig. 23,
 937 bottom right). So, we recalculate positions of the modules so that all the hits are laying on the
 938 same smooth track (Fig. 24, top left). But these recalculated positions still do not coincide with
 939 the actual positions (Fig. 24, top right). Then we record more and more tracks (Fig. 24, middle
 940 left and right). We take into account them all and determine the alignment parameters with
 941 necessary precision (Fig. 24, bottom left and right).

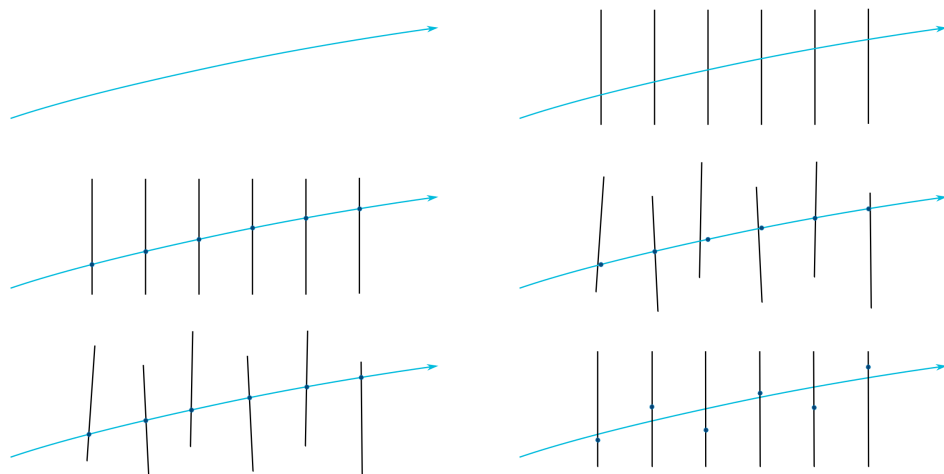


Figure 23: The alignment of a toy tracker, part 1.

946 When we record a track with a not-aligned tracker, we see that the track is not smooth. But

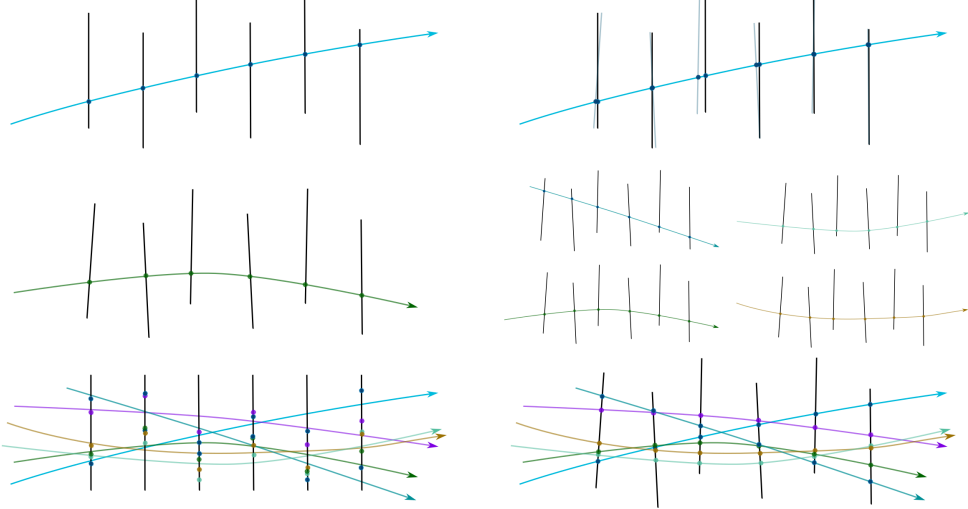


Figure 24: The alignment of a toy tracker, part 2.

that is because our knowledge of module positions is not exact. Thus, we can correct the positions assuming the track is smooth. But when we process the next track, we may find out that the positions have to be corrected again. Thus, we record many tracks and minimize residuals between measured and predicted hits.

The CMS tracker contains 1440 silicon pixel modules in PXB and PXF and 15148 silicon strip modules in TIB, TOB, TID, TEC.

The tracker alignment problem is the least squared problem. The expression to minimize is the following:

$$\chi^2(\mathbf{p}, \mathbf{q}) = \sum_j^{\text{tracks}} \sum_i^{\text{tracks}} \left(\frac{m_{ij} - f_{ij}(\mathbf{p}, \mathbf{q}_j)}{\sigma_{ij}} \right)^2 \quad (34)$$

where \mathbf{p} are parameters describing the tracker geometry, \mathbf{q}_j are parameters of the j^{th} track, $m_{ij} - f_{ij}$ are residuals, distances between the measured hit and a position predicted by the track fit, σ_{ij} is the Gaussian error of the measurement.

We can align the large substructures and individual modules with respect to their substructures. The parameters to align large substructures include their positions and orientations of the subdetectors (rotations). Thus, each subsystem is described by six parameters: three coordinates X, Y, Z and three angles α , β , γ . At the module level, we align positions and rotations with respect to the position s and angles of the corresponding large structure (Fig. 25). In addition, at the module level we align for surface deformations which are described by three parameters per sensor (Fig. 26).

A track can be described with five parameters.

We have two alignment algorithms: Millepede and HIP. Millepede performs a simultaneous fit of all alignment parameters and all track parameters while HIP perform iterative fits of alignment parameters \mathbf{p} and track parameters \mathbf{q}_j .

It is important to use different sorts of tracks for the alignment. Cosmic tracks pass through the detector vertically and do not allow us to connect different subdetectors to one another.

977 Collision tracks originate from the collision point and go in all directions. However, those tracks
 978 which cross TEC are all almost collinear and, therefore, it is difficult to measure z -coordinate of
 979 TEC modules with collision tracks only.

980

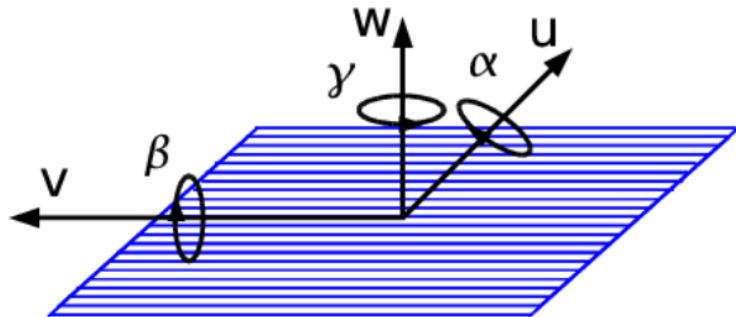


Figure 25: Alignment parameters.

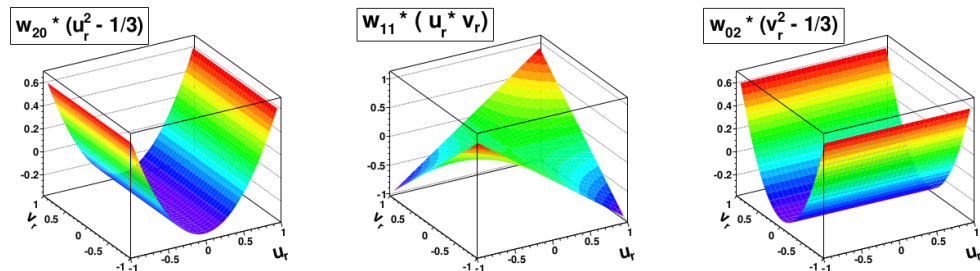


Figure 26: Surface deformations.

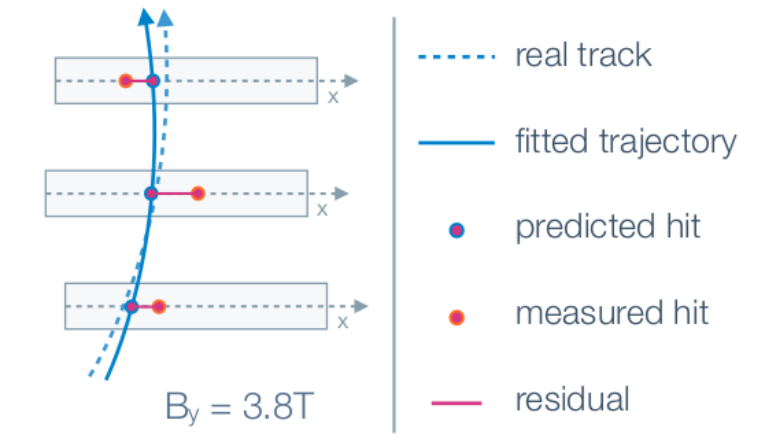


Figure 27: Track residuals.



Figure 28: Track residuals.

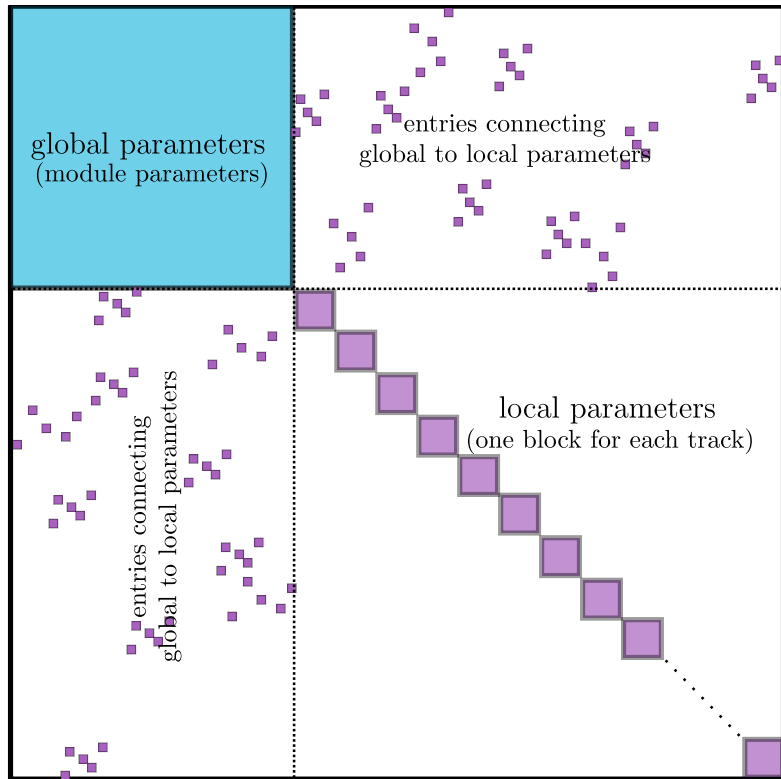


Figure 29: Track residuals.

4.2 Selected Results

CRUZET, CRAFT and first collisions of 2015

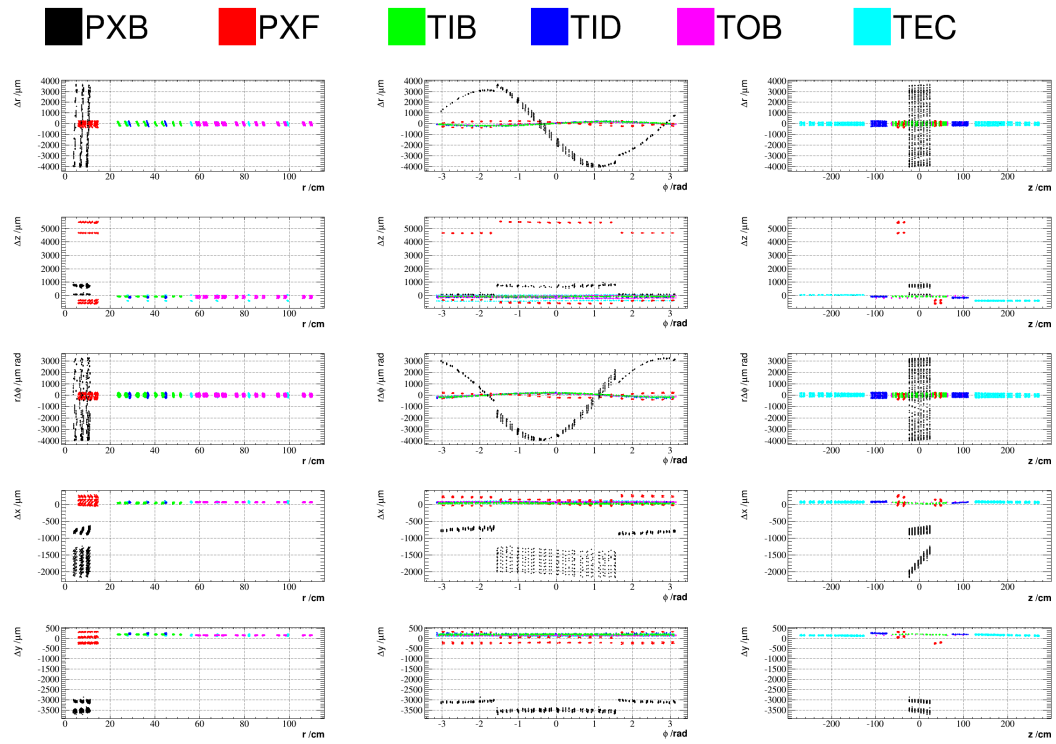


Figure 30: Geometry comparison plot of CRUZET 2015 object vs Run I.

5 $W\gamma$ Cross Section Measurement

983 Place analysis outline here

985 References

- 986 [1] Griffiths textbook
987 [2] website: <http://www.isgtw.org/spotlight/go-particle-quest-first-cern-hackfest>
988 [3] CMS Paper about Higgs boson discovery
989 [4] ATLAS Paper about Higgs boson discovery
990 [5] website: <https://mstwpdf.hepforge.org/>
991 [6] Pich lectures: The Standard Model of Electroweak interactions
992 [7] PDG
993 [8] Halzen, Martin "Quarks and leptons"
994 [9] <http://iopscience.iop.org/article/10.1088/0034-4885/70/1/R02>
995 [10] Peskin, Schroeder
996 [11] Lindsey's thesis (CMS Zg- ζ llg, 7 TeV)
997 [12] website: https://www-d0.fnal.gov/results/publications_talks/thesis/snyder/html/node17.html
998 [13] website: https://en.wikipedia.org/wiki/Cross_section_%28physics%29
999 [14] LO (1969) theory paper
1000 [15] NNLO theory paper
1001 [16] NLO theory paper
1002 [17] aTGC paper
1003 [18] Senka's thesis (CMS Wg- ζ munug, 7 TeV)
1004 [19] D0 Combination of $W\gamma$, WW, WZ and VW using 8.6 fb-1 of 2 TeV $p\bar{p}$ collisions Phys.Lett.
1005 B718 (2012) 451-459
1006 [20] LEP Combination of WW and single W using 0.7 fb-1 per experiment of e^+e^- collisions at
1007 WW pair production energies arXiv:1302.3415
1008 [21] 7TeV Wg ATLAS paper
1009 [22] ATLAS WW using 20.3 fb-1 of 8 TeV pp collisions Submitted to JHEP
1010 [23] ATLAS VW ($V=W,Z \rightarrow jj$) using 4.6 fb-1 of 7 TeV pp collisions JHEP 01 (2015) 049
1011 [24] website: https://twiki.cern.ch/twiki/bin/view/CMSPublic/PhysicsResultsSMPaTGC#Figure_1_Limits_on_WW
1012 [25] 7TeV Wg CMS paper
1013 [26] CMS WW using 4.9 fb-1 of 7 TeV pp collisions Eur. Phys. J. C 73 (2013) 2610
1014 [27] CMS WW using 19.4 fb-1 of 8 TeV pp collisions Submitted to EPJC
1015 [28] CMS VW ($V=W,Z \rightarrow jj$) using 5.0 fb-1 of 7 TeV pp collisions Eur.Phys.J. C73 (2013) 2283
1016 [29] CMS 8 TeV WW lnlnmu
1017 [30] CMS 7 TeV Zg nunug
1018 [31] CERN brochure, <http://cds.cern.ch/record/1165534/files/CERN-Brochure-2009-003-Eng.pdf>

- 1020 [32] LHC TDR
- 1021 [33] website: <http://home.cern/topics/large-hadron-collider>
- 1022 [34] website: <http://cds.cern.ch/record/1621583/files/>
- 1023 [35] http://home.cern/sites/home.web.cern.ch/files/image/update-for_cern_people/2016/06/intlumirunall_image.png
- 1024
- 1025 [36] website: <http://cds.cern.ch/journal/CERNBulletin/2014/24/News%20Articles/1706606>
- 1026 [37] website: <https://twiki.cern.ch/twiki/bin/view/CMSPublic/LumiPublicResults>